NJC

ROYAL SOCIETY OF CHEMISTRY

PAPER

View Article Online
View Journal

Published on 07 February 2025. Downloaded by Universitat Erlangen Nurnberg on 2/7/2025 3:13:54 PM.

Check for updates

Cite this: DOI: 10.1039/d5nj00043b

New bis-pyrazolate zinc(II) complexes as potential anticancer drugs: from structure to anticancer activity†

Rušid Hasić,[a] Majda Kolenović Serezlić,[a] Angelina Caković,[b] Jovana Bogojeski,[b] Danijela Nikodijević,[b] Milena Milutinović,[b] Aleksandra Stanojević,[c] Milena Čavić,[c] Andrei V. Egorov,[d] Andrei V. Komolkin,[d] Ilya V. Kornyakov,[d] Andreas Scheurer,[e] Ralph Puchta[efgh] and Tanja V. Soldatović *[a]

Received 4th January 2025,
Accepted 29th January 2025

DOI: 10.1039/d5nj00043b

rsc.li/njc

Three novel Zn(II) complexes **[ZnCl$_2$(H$_2$L^{tBu})]**, **[ZnCl$_2$(Me$_2$L^{tBu})]** and **[Zn$_2$Cl$_4$(H$_2$L^{CatBiPyPh})$_2$]** (where H$_2$L^{tBu} is 2,6-bis(5-*tert*-butyl-1*H*-pyrazol-3-yl)pyridine, Me$_2$L^{tBu} is 2,6-bis(5-*tert*-butyl-1-methyl-1*H*-pyrazol-3-yl)pyridine and H$_2$L^{CatBiPyrPh} is 1,2-bis((5-phenyl-1*H*-pyrazol-3-yl)methoxy)benzene) were synthesized and characterized using various spectroscopic techniques, including UV-vis, IR, ^{1}D (^{1}H and ^{13}C) and 2D (^{1}H–^{1}H COSY) NMR. The structures of complexes **[ZnCl$_2$(H$_2$L^{tBu})]** and **[Zn$_2$Cl$_4$(H$_2$L^{CatBiPyPh})$_2$]** were elucidated through X-ray crystallography. The interactions of the complexes with CT-DNA and human serum albumin (HSA) were investigated using UV-vis spectroscopy and fluorescence emission titration. All examined complexes exhibited quenching constant, K_{sv}, values in the order of 10^4 with CT-DNA. Constant values followed the trend **[ZnCl$_2$(Me$_2$L^{tBu})]** < **[Zn$_2$Cl$_4$(H$_2$L^{CatBiPyPh})$_2$]** < **[ZnCl$_2$(H$_2$L^{tBu})]**. The results indicated a moderate interaction between the complexes and HSA. In terms of cytotoxic activity, the zinc(II) complexes significantly decreased the viability of colon (HCT-116) and pancreatic (MIA PaCa-2) cancer cell lines, where the effect on pancreatic cells after 72 h is especially emphasized. The most pronounced occurrence of apoptosis, as the dominant type of complex-induced cell death, was associated with complex **[ZnCl$_2$(H$_2$L^{tBu})]**, while necrosis was observed at lower percentages in all investigated treatments. All complexes demonstrated downregulation of the tumor suppressor gene *TP53* (*homo sapiens* tumor protein p53). Treatment with **[ZnCl$_2$(H$_2$L^{tBu})]** resulted in downregulation of *TP53*, *CASP3* (*Caspase 3*) and *IGF1R* (insulin-like growth factor 1), potentially impairing the effective apoptotic process and reducing cell proliferation.

Introduction

Over the last century, platinum-based complexes have been used as anticancer drugs.[1,2] However, side effects, such as cell-acquired resistance and high toxicity,[3] have prompted investigation of other metal complexes.[4,5] The rising incidence of digestive tract carcinoma demands special attention. Colorectal and pancreatic carcinomas, in particular, are not only becoming more frequent but also rank among the most aggressive forms of cancer. This highlights the importance of research on model systems for these diseases. HCT-116 colorectal cancer cells and MIA PaCa-2 pancreatic cancer cells are commonly used as representative models. Such research aims to identify novel, specific substances suitable for treating these challenging conditions.[6–8]

The importance of zinc in biological systems is definitively related to its unique chemical features: Zn(II) is redox inactive,

[a] Department of Natural-Mathematical Sciences, State University of Novi Pazar, Vuka Karadžića 9, 36300 Novi Pazar, Serbia. E-mail: tsoldatovic@np.ac.rs; Fax: +381(0)20-337-0669; Tel: +381(0)20-317-754
[b] Faculty of Science, University of Kragujevac, Radoja Domanovića 12, 34000 Kragujevac, Serbia
[c] Department of Experimental Oncology, Institute for Oncology and Radiology of Serbia, Pasterova 14, 11000 Belgrade, Serbia
[d] St. Petersburg State University, 7/9 Universitetskaya nab., 199034, St. Petersburg, Russia
[e] Inorganic Chemistry, Department of Chemistry and Pharmacy, University of Erlangen-Nürnberg, Egerlandstrasse 1, 91058 Erlangen, Germany
[f] Staatliche Fachoberschule Nürnberg, Lothar-von-Faber-Schule, Schafhofstr. 25, 90411 Nürnberg, Germany
[g] University of Erlangen-Nuremberg, Department of Chemistry and Pharmacy, Computer Chemistry Center, Nägelsbachstr. 25, 91052 Erlangen, Germany
[h] University of Erlangen-Nuremberg, Zentralinstitute for Scientific Computing (ZISC), Martensstr. 5a, 91058 Erlangen, Germany

† Electronic supplementary information (ESI) available. CCDC 2339722 and 2339723. For ESI and crystallographic data in CIF or other electronic format see DOI: https://doi.org/10.1039/d5nj00043b

Published on 07 February 2025. Downloaded by Universitat Erlangen Nurnberg on 2/7/2025 3:13:54 PM.

is a strong Lewis acid, has a d^{10} configuration, is diamagnetic, can support a variable coordination geometry and is prone to a fast exchange of ligands. Its electron affinity resembles that of copper or nickel, but the lack of redox activity of the divalent zinc ion, differently from copper or iron, eliminates any chances of free radical reactions and makes it crucial for the body's antioxidant protection system.[9]

The vital importance of zinc(II) ions can be easily understood considering that this metal is present in more than 3000 human proteins including nucleic acid binding proteins; is involved in the catalytic activity of thousands of enzymes; and plays a role in DNA synthesis, protein synthesis and immune functions.[10,11] It is also essential for synaptic plasticity and normal brain activity.[12,13] The binding of Zn(II) with catalytic and/or structural sites of a large number of proteins is a key-factor in determining their conformations.[14] Many studies evidenced that the impairment of Zn(II) homeostasis can lead to its involvement in triggering and developing different cancer diseases. In the case of an excess of cellular zinc(II) a chelation therapy approach has been suggested[15,16] whereas in the case of Zn(II) deficiency, as in prostate cancer, the use of ionophore ligands able to restore the suitable Zn(II) concentration has been pursued.[17] The biological prominence of zinc(II) ions and emerging insights into zinc biology are the outcomes of techniques and methods progressively developed in the last several years.

Zinc(II) ions have an affinity to coordinate both nitrogen or oxygen donor atoms in biomolecules.[18,19] Our recent studies indicate that heteronuclear complexes with adopted general formula *cis*- or *trans*-Pt-L-Zn are more reactive toward DNA constituents than sulfur-containing biomolecules. These complexes have demonstrated significantly higher cytotoxicity compared to cisplatin.[20,21] The increased cytotoxicity may be attributed to potential interference with multiple intracellular processes and structures that incorporate the zinc(II) ion. The molecular mechanisms governing the response of the colorectal cancer cell line HCT116 to the cytotoxic action of these complexes appear to be complex, involving intricate interplays between various signaling pathways.[20–22]

Proper choice of ligands surrounding a metal center is crucial, as they affect the reactivity and lipophilicity of a complex, due to their ability to stabilize specific oxidation states and to impart substitution inertness.[23] Metal complexes of bis-pyrazolylpyridine ligands are the subject of intensive research, because of their rich coordination chemistry, and a number of established and potential application areas, including medicinal chemistry.[24] These ligands have already been used in reactions with other metals, such as Au(III), Rh(III), Ru(III), Os(II), Pd(II) and Pt(II).[22–26]

Complex Au(III) with 2,6-bis(5-*tert*-butyl-1*H*-pyrazol-3-yl)pyridine (H_2L^{tBu}) $[AuCl(H_2L^{tBu})]Cl_2$ induced perturbations of the cell cycle and led to apoptosis in human melanoma A375 cells and also affected the level of reactive oxygen species (ROS) in the same cells.[25] A novel rhodium(III) complex $[RhCl_3(H_2L^{tBu})]$ exhibited good DNA and BSA interaction ability.[26] The ruthenium(III) pincer-type complex $[RuCl_3(H_2L^{tBu})]$ has significant *in vitro* cytotoxic activity against mouse colon carcinoma CT26 cells and *in vivo* antitumor activity in murine heterotopic colon carcinoma. Also, the complex induced G0/G1 cell cycle arrest and apoptotic death in CT26 cells and showed antiproliferative activity, as evaluated by the detection of the expression levels of the Ki67 protein.[27] The results of the influence of the studied $[OsCl_2(H_2L^{tBu})H_2O]$, $[OsCl_2(Me_2L^{tBu})\text{-}H_2O]$ and $[OsCl_2(terpy)H_2O]$ (where Me_2L^{tBu} = bis(5-*tert*-butyl-1-methyl-1*H*-pyrazol-3-yl)pyridine and terpy = 2,2′:6′,2″-terpyridine) complexes on the integrity of DNA (electrophoresis test) indicate a moderate interaction of Os complexes with DNA, which, in addition to disturbing the redox balance, is one of the possible mechanisms of action of these substances because the molecular action of these complexes is not strongly dependent on interaction with DNA.[28] The results of biological testing of four new complexes $[PdCl(H_2L^{tBu})]Cl$ (Pd1), $[PtCl(H_2L^{tBu})]Cl$ (Pt1), $[PdCl(Me_2L^{tBu})]Cl$ (Pd2) and $[PtCl(Me_2L^{tBu})]Cl$ (Pt2) showed that all complexes exert moderate to highly selective cytotoxicity, inducing apoptosis and autophagy in HeLa and PANC-1 tumor cell lines. Cell cycle analysis showed that in HeLa cells Pd1, Pd2 and Pt1 induced accumulation of cells in the S phase, whereas in PANC-1 cells Pd2 and Pt1 induced G2/M cycle arrest and Pd1 induced G0/G1 arrest.[29]

Based on the coordination ability of bis-pyrazolyl pyridine ligands, we designed, synthesized and characterized the three new monofunctional Zn(II) complexes with bispyrazolate ligands such as 2,6-bis(5-*tert*-butyl-1*H*-pyrazol-3-yl)pyridine (H_2L^{tBu}), 2,6-bis(5-*tert*-butyl-1-methyl-1*H*-pyrazol-3-yl)pyridine (Me_2L^{tBu}), and 1,2-bis((5-phenyl-1*H*-pyrazol-3-yl)methoxy)benzene ($H_2L^{CatBiPyrPh}$) (Fig. 1). These novel zinc(II) complexes would be particularly significant because they could address key limitations of current zinc-based anticancer agents, including low selectivity, poor bioavailability, and limited efficacy in targeting specific biomolecules. The distinctive design of these zinc(II) complexes, incorporating bis-pyrazolyl ligands, would enhance their structural flexibility and coordination properties, potentially improving their interaction with biomolecular targets implicated in cancer progression. By overcoming these challenges, these complexes could hold promise for the development of more effective and selective cancer therapies.

Different experimental methods were used to evaluate their antitumor activity and coordination ability.

Results and discussion

Synthesis and structure of complexes

Novel zinc(II) complexes $\mathbf{[ZnCl_2(H_2L^{tBu})]}$, $\mathbf{[ZnCl_2(Me_2L^{tBu})]}$ and $\mathbf{[Zn_2Cl_4(H_2L^{CatBiPyPh})_2]}$ were synthesized by dissolving an equimolar amount of the zinc salt (anhydrous $ZnCl_2$), and ligands H_2L^{tBu}, Me_2L^{tBu} and $H_2L^{CatBiPyPh}$ in ethanol. The solutions of ligands were drop-wise added to the solution of the zinc salt and left to stir overnight at room temperature. The obtained white participates were filtered and characterized. The synthesis of the complexes is outlined in Scheme 1.

The synthesized zinc(II) complexes were characterized by elemental analysis and various spectroscopy techniques such

 This journal is © The Royal Society of Chemistry and the Centre National de la Recherche Scientifique 2025

Published on 07 February 2025. Downloaded by Universitat Erlangen Nurnberg on 2/7/2025 3:13:54 PM.

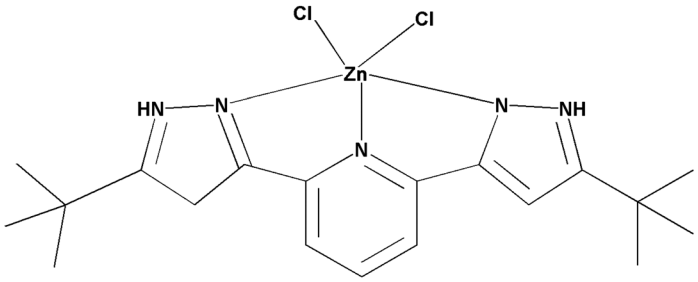

$[ZnCl_2(H_2L^{tBu})]$

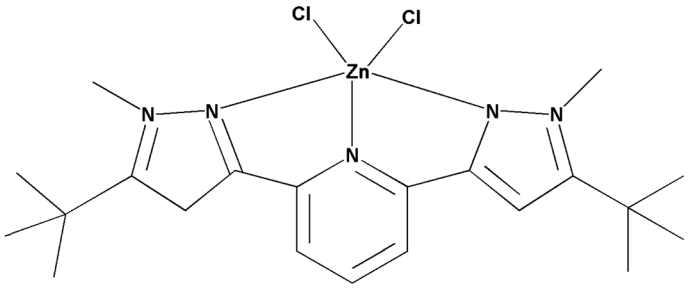

$[ZnCl_2(Me_2L^{tBu})]$

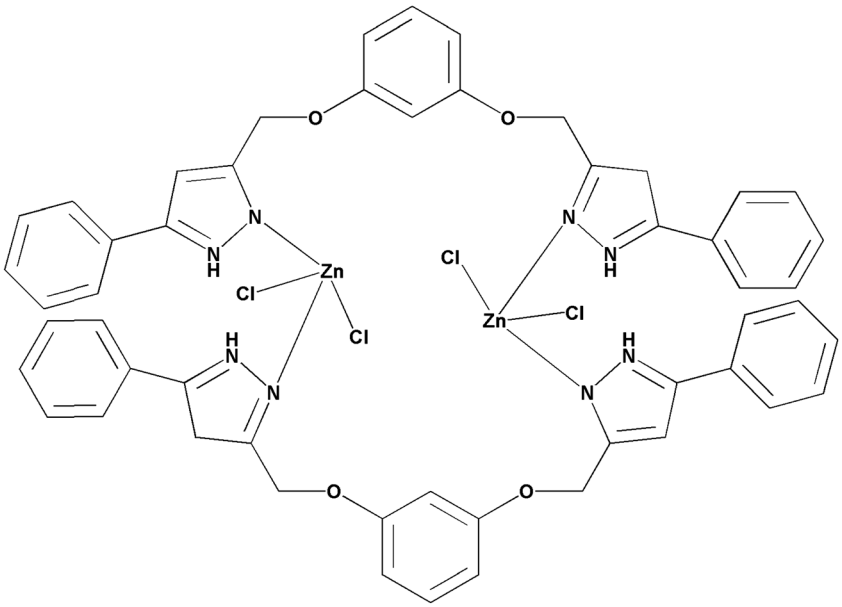

$[Zn_2Cl_4(H_2L^{CatBiPyPh})_2]$

Fig. 1 Structures of the investigated zinc(II) complexes.

as UV-vis, IR, ^{1}D (^{1}H and ^{13}C) and 2D (^{1}H–^{1}H COSY) and NMR (see the Experimental section). The single crystals of $[ZnCl_2(H_2L^{tBu})]$ and $[Zn_2Cl_4(H_2L^{CatBiPyPh})_2]$ complexes were suitable for X-ray analysis. The characterization of the $[ZnCl_2(Me_2L^{tBu})]$ complex was not possible because blocked crystals were formed, but the results of NMR characterization indicated that only a distinct species was formed, with the shifted set of signals for the pyrazole and pyridine moieties, when compared to the free ligand signals.

Crystal structure discussion

The complex $[ZnCl_2(H_2L^{tBu})]$ crystallizes in the triclinic crystal system and the $P\bar{1}$ space group. Its molecular structure is shown in Fig. 2 and the corresponding geometric parameters

Published on 07 February 2025. Downloaded by Universitat Erlangen Nurnberg on 2/7/2025 3:13:54 PM.

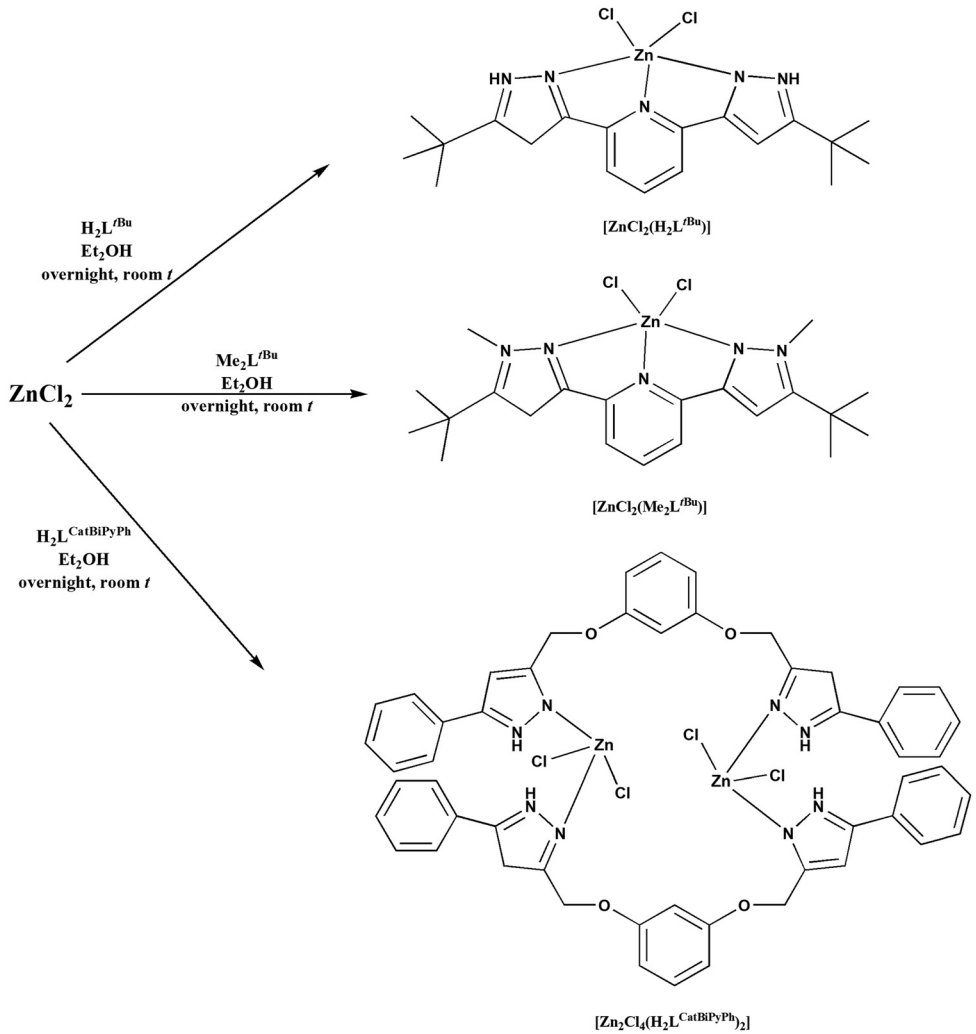

Scheme 1 Synthetic pathways for the preparation of complexes.

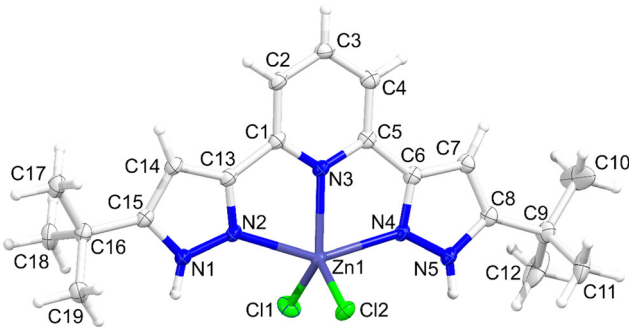

Fig. 2 The ORTEP representation of the molecular structure of the complex **[ZnCl$_2$(H$_2$L^{tBu})]** with atomic labeling. Thermal ellipsoids are at the 50% probability level.

are collected in Table 1. The Zn(II) ion is five-coordinated with the tridentate *N*,*N*,*N*-donor and two chlorido ligands. The degree of trigonality[30] is 0.507 indicating a strong shift to a distorted trigonal bipyramidal geometry (for a perfectly trigonal bipyramidal polyhedron the degree of trigonality is equal to unity, while it becomes zero for a perfect square pyramidal polyhedron). Due to tridentate coordination of the *N*,*N*,*N*-donor the N3 nitrogen atom is located closer to the Zn(II) ion than N2 and N4 nitrogen atoms and the N4–Zn1–N2 bond angle is about 148°. The *N*,*N*,*N*-donor ligand skeleton is essentially planar.

The complex **[Zn$_2$Cl$_4$(H$_2$L^{CatBiPyPh})$_2$]** crystallizes in the triclinic crystal system and the $P\bar{1}$ space group. Its molecular structure is shown in Fig. 3 and the corresponding geometric parameters are collected in Table 2. The complex consists of two parts which are related by an inversion center and its formula is $Zn_2Cl_4C_{52}N_8O_4H_{44}\cdot1.73H_2O$. The Zn(II) ion is four-coordinated by two nitrogen atoms and two chlorido ligands. The values of bond angles Cl2A–Zn1–Cl1, N1–Zn1–Cl1, N1–Zn1–Cl2A, N1–Zn1–N3, N3–Zn1–Cl1, and N3–Zn1–Cl2A are close to 109.47°, which indicates that the surrounding geometry of the Zn(II) ion is a distorted tetrahedron.

Zinc(II) is a versatile metal ion capable of adopting various coordination geometries depending on its environment and the nature of the donor sites of the involved ligands. Its electron configuration of $3d^{10}$ indicates fully filled d-orbitals, which

 This journal is © The Royal Society of Chemistry and the Centre National de la Recherche Scientifique 2025

Published on 07 February 2025. Downloaded by Universitat Erlangen Nurnberg on 2/7/2025 3:13:54 PM.

Table 1 Geometric parameters for the complex **[$ZnCl_2(H_2L^{tBu})$]**

Bond lengths [Å]			
Zn1–Cl1	2.2724 (5)	C3–C4	1.396 (3)
Zn1–Cl2	2.2774 (5)	C4–C5	1.389 (3)
Zn1–N2	2.2269 (16)	C5–C6	1.471 (3)
Zn1–N3	2.1049 (15)	C6–C7	1.395 (3)
Zn1–N4	2.1835 (16)	C7–C8	1.387 (3)
N1–N2	1.341 (2)	C8–C9	1.513 (3)
N1–C15	1.358 (2)	C9–C10	1.518 (4)
N2–C13	1.337 (2)	C9–C11	1.532 (3)
N3–C1	1.349 (2)	C9–C12	1.520 (3)
N3–C5	1.343 (3)	C13–C14	1.401 (3)
N4–N5	1.349 (2)	C14–C15	1.389 (3)
N4–C6	1.340 (2)	C15–C16	1.507 (3)
N5–C8	1.352 (3)	C16–C17	1.528 (3)
C1–C2	1.391 (3)	C16–C18	1.539 (3)
C1–C13	1.462 (3)	C16–C19	1.532 (3)
C2–C3	1.384 (3)		
Bond angles [°]			
Cl1–Zn1–Cl2	118.25 (2)	N3–C5–C6	113.95 (16)
N2–Zn1–Cl1	99.19 (5)	C4–C5–C6	124.45 (18)
N2–Zn1–Cl2	94.68 (4)	N4–C6–C5	116.20 (17)
N3–Zn1–Cl1	125.39 (4)	N4–C6–C7	111.06 (16)
N3–Zn1–Cl2	116.31 (4)	C7–C6–C5	132.74 (18)
N3–Zn1–N2	73.99 (6)	C8–C7–C6	105.29 (17)
N3–Zn1–N4	74.89 (6)	N5–C8–C7	106.23 (17)
N4–Zn1–Cl1	96.25 (4)	N5–C8–C9	122.44 (17)
N4–Zn1–Cl2	101.69 (4)	C7–C8–C9	131.32 (18)
N4–Zn1–N2	148.74 (6)	C8–C9–C10	108.73 (18)
N2–N1–C15	112.98 (16)	C8–C9–C11	109.76 (17)
N1–N2–Zn1	139.96 (12)	C8–C9–C12	110.13 (19)
C13–N2–Zn1	114.94 (13)	C10–C9–C11	108.5 (3)
C13–N2–N1	105.11 (15)	C10–C9–C12	111.2 (3)
C1–N3–Zn1	120.24 (13)	C12–C9–C11	108.46 (19)
C5–N3–Zn1	119.42 (12)	N2–C13–C1	116.64 (17)
C5–N3–C1	120.34 (16)	N2–C13–C14	110.94 (17)
N5–N4–Zn1	139.47 (12)	C14–C13–C1	132.31 (17)
C6–N4–Zn1	115.51 (12)	C15–C14–C13	105.47 (16)
C6–N4–N5	105.00 (15)	N1–C15–C14	105.48 (17)
N4–N5–H5	123.8	N1–C15–C16	122.69 (17)
N4–N5–C8	112.40 (15)	C14–C15–C16	131.52 (17)
N3–C1–C2	121.22 (19)	C15–C16–C17	109.22 (17)
N3–C1–C13	113.89 (16)	C15–C16–C18	109.39 (16)
C2–C1–C13	124.82 (17)	C15–C16–C19	110.77 (16)
C3–C2–C1	118.30 (18)	C17–C16–C18	108.51 (17)
C2–C3–C4	120.48 (18)	C17–C16–C19	110.74 (17)
C5–C4–C3	117.92 (19)	C19–C16–C18	108.18 (17)
N3–C5–C4	121.60 (17)		
Torsion angles [°]			
Zn1–N2–C13–C1	3.7 (2)	N5–C8–C9–C12	52.9 (3)
Zn1–N2–C13–C14	−179.69 (13)	C1–N3–C5–C4	−2.3 (3)
Zn1–N3–C1–C2	178.26 (14)	C1–N3–C5–C6	178.07 (16)
Zn1–N3–C1–C13	−4.6 (2)	C1–C2–C3–C4	−2.4 (3)
Zn1–N3–C5–C4	178.09 (14)	C1–C13–C14–C15	175.0 (2)
Zn1–N3–C5–C6	−1.5 (2)	C2–C1–C13–N2	177.35 (18)
Zn1–N4–N5–C8	178.98 (14)	C2–C1–C13–C14	1.6 (3)
Zn1–N4–C6–C5	0.6 (2)	C2–C3–C4–C5	−1.0 (3)
Zn1–N4–C6–C7	−179.39 (12)	C3–C4–C5–N3	3.5 (3)
N1–N2–C13–C1	−176.27 (16)	C3–C4–C5–C6	−176.97 (17)
N1–N2–C13–C14	0.3 (2)	C4–C5–C6–N4	−179.07 (17)
N1–C15–C16–C17	165.02 (18)	C4–C5–C6–C7	1.0 (3)
N1–C15–C16–C18	−76.4 (2)	C5–N3–C1–C2	−1.3 (3)
N1–C15–C16–C19	42.8 (2)	C5–N3–C1–C13	175.86 (16)
N2–N1–C15–C14	−1.0 (2)	C5–C6–C7–C8	−179.68 (19)
N2–N1–C15–C16	173.31 (16)	C6–N4–N5–C8	0.7 (2)
N2–C13–C14–C15	−0.9 (2)	C6–C7–C8–N5	0.1 (2)
N3–C1–C2–C3	3.6 (3)	C6–C7–C8–C9	−179.2 (2)
N3–C1–C13–N2	0.3 (2)	C7–C8–C9–C10	−5.9 (4)
N3–C1–C13–C14	−175.44 (19)	C7–C8–C9–C11	112.7 (3)
N3–C5–C6–N4	0.5 (2)	C7–C8–C9–C12	−128.0 (2)
N3–C5–C6–C7	−179.44 (19)	C13–C1–C2–C3	−173.23 (18)
N4–N5–C8–C7	−0.5 (2)	C13–C14–C15–N1	1.1 (2)
N4–N5–C8–C9	178.83 (17)	C13–C14–C15–C16	−172.48 (19)

Table 1 (*continued*)

N4–C6–C7–C8	0.3 (2)	C14–C15–C16–C17	−22.3 (3)
N5–N4–C6–C5	179.38 (15)	C14–C15–C16–C18	96.3 (2)
N5–N4–C6–C7	−0.6 (2)	C14–C15–C16–C19	−144.5 (2)
N5–C8–C9–C10	175.0 (3)	C15–N1–N2–Zn1	−179.52 (15)
N5–C8–C9–C11	−66.5 (3)	C15–N1–N2–C13	0.4 (2)

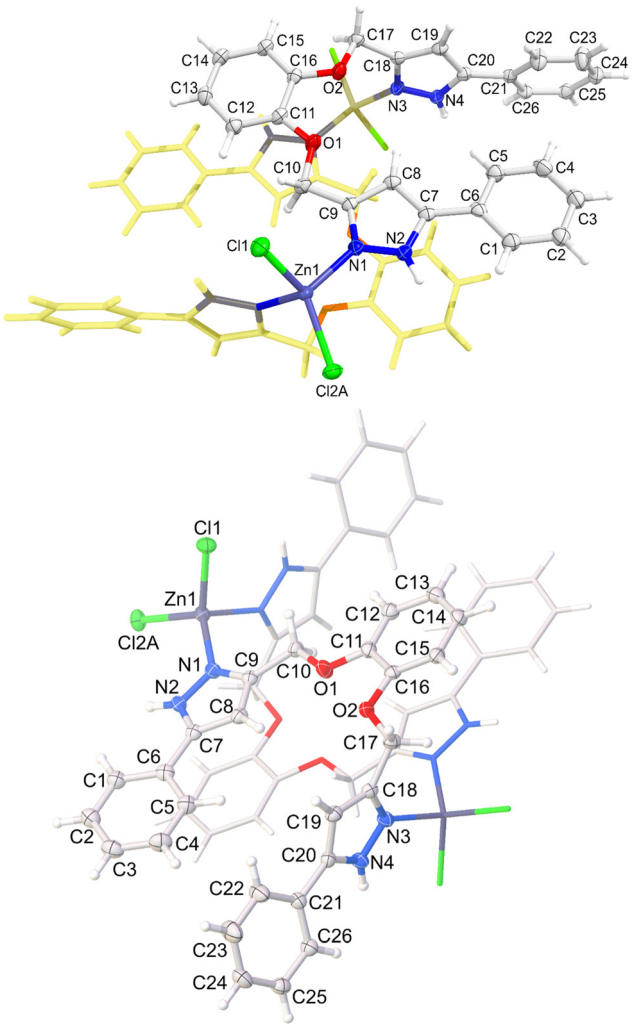

Fig. 3 The ORTEP representation of the molecular structure of the complex **[$Zn_2Cl_4(H_2L^{CatBiPyPh})_2$]** with atomic labeling. Disorder is not shown for the sake of clarity. Thermal ellipsoids are at the 50% probability level.

contributes to its ability to form stable complexes with a diverse array of ligands through both ionic and covalent interactions. Common coordination numbers for zinc(II) typically include 4, 5, and 6, corresponding to tetrahedral, trigonal bipyramidal (or square pyramidal), and octahedral geometries, respectively.

The flexibility of the H_2L^{tBu} chelating ligand allowed zinc(II) to stabilize a five-coordinate structure in a trigonal bipyramidal configuration. This geometry is favored due to the ability of the tridentate ligand to form a stable chelate ring, which enhance thermodynamic stability through the chelate effect. In contrast,

Published on 07 February 2025. Downloaded by Universitat Erlangen Nurnberg on 2/7/2025 3:13:54 PM.

Table 2 Geometric parameters for the complex $[Zn_2Cl_4(H_2L^{CatBiPyPh})_2]$

Bond lengths [Å]			
Zn1–Cl1	2.2289 (7)	C6–C7	1.472 (4)
Zn1–Cl2A	2.2201 (8)	C7–C8	1.386 (4)
Zn1–N1	2.028 (2)	C8–C9	1.390 (4)
Zn1–N3^{i}	2.032 (2)	C9–C10	1.500 (4)
O1–C10	1.421 (3)	C11–C12	1.383 (4)
O1–C11	1.369 (3)	C11–C16	1.404 (4)
O2–C16	1.379 (3)	C12–C13	1.395 (4)
O2–C17	1.436 (3)	C13–C14	1.381 (4)
N1–N2	1.361 (3)	C14–C15	1.397 (4)
N1–C9	1.340 (3)	C15–C16	1.377 (4)
N2–C7	1.352 (3)	C17–C18	1.490 (4)
N3–N4	1.350 (3)	C18–C19	1.396 (4)
N3–C18	1.338 (3)	C19–C20	1.392 (4)
N4–C20	1.351 (3)	C20–C21	1.466 (4)
C1–C2	1.391 (4)	C21–C22	1.384 (4)
C1–C6	1.393 (4)	C21–C26	1.391 (4)
C2–C3	1.383 (4)	C22–C23	1.382 (4)
C3–C4	1.385 (5)	C23–C24	1.383 (5)
C4–C5	1.392 (4)	C24–C25	1.385 (4)
C5–C6	1.400 (4)	C25–C26	1.387 (4)
Bond angles [°]			
Cl2A–Zn1–Cl1	114.74 (5)	C8–C9–C10	127.0 (2)
N1–Zn1–Cl1	109.03 (6)	O1–C10–C9	103.5 (2)
N1–Zn1–Cl2A	115.21 (8)	O1–C11–C12	125.8 (3)
N1–Zn1–N3^{i}	107.79 (9)	O1–C11–C16	113.8 (2)
N3^{i}–Zn1–Cl1	103.19 (6)	C12–C11–C16	120.3 (2)
N3^{i}–Zn1–Cl2A	105.90 (7)	C11–C12–C13	119.2 (3)
C11–O1–C10	120.0 (2)	C14–C13–C12	120.5 (3)
C16–O2–C17	117.5 (2)	C13–C14–C15	120.1 (3)
N2–N1–Zn1	125.02 (17)	C16–C15–C14	119.8 (3)
C9–N1–Zn1	128.34 (18)	O2–C16–C11	114.0 (2)
C9–N1–N2	105.5 (2)	C15–C16–O2	126.0 (3)
C7–N2–N1	111.5 (2)	C15–C16–C11	120.0 (3)
N4–N3–Zn1^{i}	120.95 (16)	O2–C17–C18	107.0 (2)
C18–N3–Zn1^{i}	131.90 (19)	N3–C18–C17	118.8 (2)
N3–N4–C20	112.2 (2)	N3–C18–C19	110.1 (2)
C2–C1–C6	120.3 (3)	C19–C18–C17	131.1 (2)
C3–C2–C1	120.2 (3)	C20–C19–C18	106.1 (2)
C2–C3–C4	120.1 (3)	N4–C20–C19	105.7 (2)
C3–C4–C5	120.1 (3)	N4–C20–C21	123.0 (2)
C4–C5–C6	120.2 (3)	C19–C20–C21	131.1 (2)
C1–C6–C5	119.1 (3)	C22–C21–C20	119.0 (2)
C1–C6–C7	122.2 (2)	C22–C21–C26	119.3 (3)
C5–C6–C7	118.7 (2)	C26–C21–C20	121.7 (2)
N2–C7–C6	123.8 (2)	C23–C22–C21	120.5 (3)
N2–C7–C8	106.4 (2)	C22–C23–C24	120.3 (3)
C8–C7–C6	129.8 (3)	C23–C24–C25	119.4 (3)
C7–C8–C9	105.9 (2)	C24–C25–C26	120.4 (3)
N1–C9–C8	110.6 (2)	C25–C26–C21	120.0 (2)
N1–C9–C10	122.4 (2)		
Torsion angles [°]			
Zn1–N1–N2–C7	−169.76 (16)	C6–C1–C2–C3	−0.1 (4)
Zn1–N1–C9–C8	168.53 (17)	C6–C7–C8–C9	179.0 (2)
Zn1–N1–C9–C10	−13.2 (3)	C7–C8–C9–N1	0.6 (3)
Zn1^{i}–N3–N4–C20	168.74 (18)	C7–C8–C9–C10	−177.6 (2)
Zn1^{i}–N3–C18–C17	12.4 (4)	C8–C9–C10–O1	−1.3 (3)
Zn1^{i}–N3–C18–C19	−167.67 (19)	C9–N1–N2–C7	−0.9 (3)
O1–C11–C12–C13	179.4 (2)	C10–O1–C11–C12	−1.6 (4)
O1–C11–C16–O2	−0.3 (3)	C10–O1–C11–C16	178.6 (2)
O1–C11–C16–C15	−178.1 (2)	C11–O1–C10–C9	−176.8 (2)
O2–C17–C18–N3	84.6 (3)	C11–C12–C13–C14	0.1 (4)
O2–C17–C18–C19	−95.3 (3)	C12–C11–C16–O2	179.8 (2)
N1–N2–C7–C6	−178.8 (2)	C12–C11–C16–C15	2.0 (4)
N1–N2–C7–C8	1.2 (3)	C12–C13–C14–C15	−0.7 (4)
N1–C9–C10–O1	−179.3 (2)	C13–C14–C15–C16	2.0 (4)
N2–N1–C9–C8	0.2 (3)	C14–C15–C16–O2	179.9 (2)
N2–N1–C9–C10	178.5 (2)	C14–C15–C16–C11	−2.6 (4)
N2–C7–C8–C9	−1.1 (3)	C16–O2–C17–C18	−147.5 (2)
N3–N4–C20–C19	0.6 (3)	C16–C11–C12–C13	−0.7 (4)
N3–N4–C20–C21	−176.2 (2)	C17–O2–C16–C11	166.3 (2)
N3–C18–C19–C20	1.2 (3)	C17–O2–C16–C15	−16.0 (3)
N4–N3–C18–C17	179.2 (2)	C17–C18–C19–C20	−178.9 (3)
N4–N3–C18–C19	−0.9 (3)	C18–N3–N4–C20	0.2 (3)
N4–C20–C21–C22	−165.1 (3)	C18–C19–C20–N4	−1.1 (3)
N4–C20–C21–C26	17.8 (4)	C18–C19–C20–C21	175.4 (3)
C1–C2–C3–C4	−0.4 (4)	C19–C20–C21–C22	18.9 (5)
C1–C6–C7–N2	−9.5 (4)	C19–C20–C21–C26	−158.2 (3)
C1–C6–C7–C8	170.4 (3)	C20–C21–C22–C23	−176.7 (3)
C2–C1–C6–C5	1.2 (4)	C20–C21–C26–C25	177.7 (2)
C2–C1–C6–C7	−179.7 (2)	C21–C22–C23–C24	−1.1 (6)
C2–C3–C4–C5	0.0 (4)	C22–C21–C26–C25	0.6 (4)
C3–C4–C5–C6	1.0 (4)	C22–C23–C24–C25	0.7 (6)
C4–C5–C6–C1	−1.6 (4)	C23–C24–C25–C26	0.4 (5)
C4–C5–C6–C7	179.3 (2)	C24–C25–C26–C21	−1.1 (4)
C5–C6–C7–N2	169.6 (2)	C26–C21–C22–C23	0.4 (5)
C5–C6–C7–C8	−10.4 (4)		

Symmetry code(s): (i) $-x + 1, -y + 1, -z + 1$.

the bulky substituents on the $H_2L^{CatBiPyPh}$ ligand create steric hindrance, potentially limiting the coordination of zinc(II) ions to four sites. This steric crowding preferentially leads to the adoption of a tetrahedral geometry, as larger substituents impeded the approach of additional donor atoms or solvent molecules, thus limiting coordination. The coordination geometry adopted by zinc(II) is critically dependent on the steric bulk, electronic donating ability, and spatial arrangement of the donor atoms within the chelating ligands. These factors influence the ligand field strength, which in turn affects the splitting of d-orbitals and the overall stability of the complexes.[18] Moreover, the chelation and steric hindrance provided by the ligands in zinc(II) complexes can effectively prevent hydrolysis. The chelate effect strengthens the coordination bond between the ligand and the zinc(II) ion, while the steric bulk, resulting from the size and spatial arrangement of the ligands, obstructs the approach of water molecules. As a result, these complexes are expected to exhibit enhanced stability and a reduced propensity for undesirable reactions under physiological conditions. Understanding these parameters is essential for predicting the reactivity and bioavailability of zinc(II) in various bioinorganic processes, particularly in relation to its mechanisms of action in anticancer activity.

DNA-binding properties

Fluorescence spectroscopy was employed to assess the intercalation capability of the tested compounds. Intercalation is a DNA binding mode where planar aromatic molecules insert between the base pairs of DNA strands, causing chain elongation. Ethidium bromide (EB) serves as a common DNA intercalator, exhibiting strong fluorescence emission at 612 nm when intercalated between DNA strands.[31–35] Compounds capable of displacing intercalated EB, by inserting themselves between DNA strands, would lead to a decrease in fluorescence emission.[35,36]

Fluorescence titrations were conducted in the presence of EB using a constant concentration of DNA/EB solution and increasing concentrations of the complexes, as shown in Fig. 4. The interaction between the complex and DNA was investigated in the presence of ethidium bromide (EB) to evaluate the

 This journal is © The Royal Society of Chemistry and the Centre National de la Recherche Scientifique 2025

Published on 07 February 2025. Downloaded by Universitat Erlangen Nurnberg on 2/7/2025 3:13:54 PM.

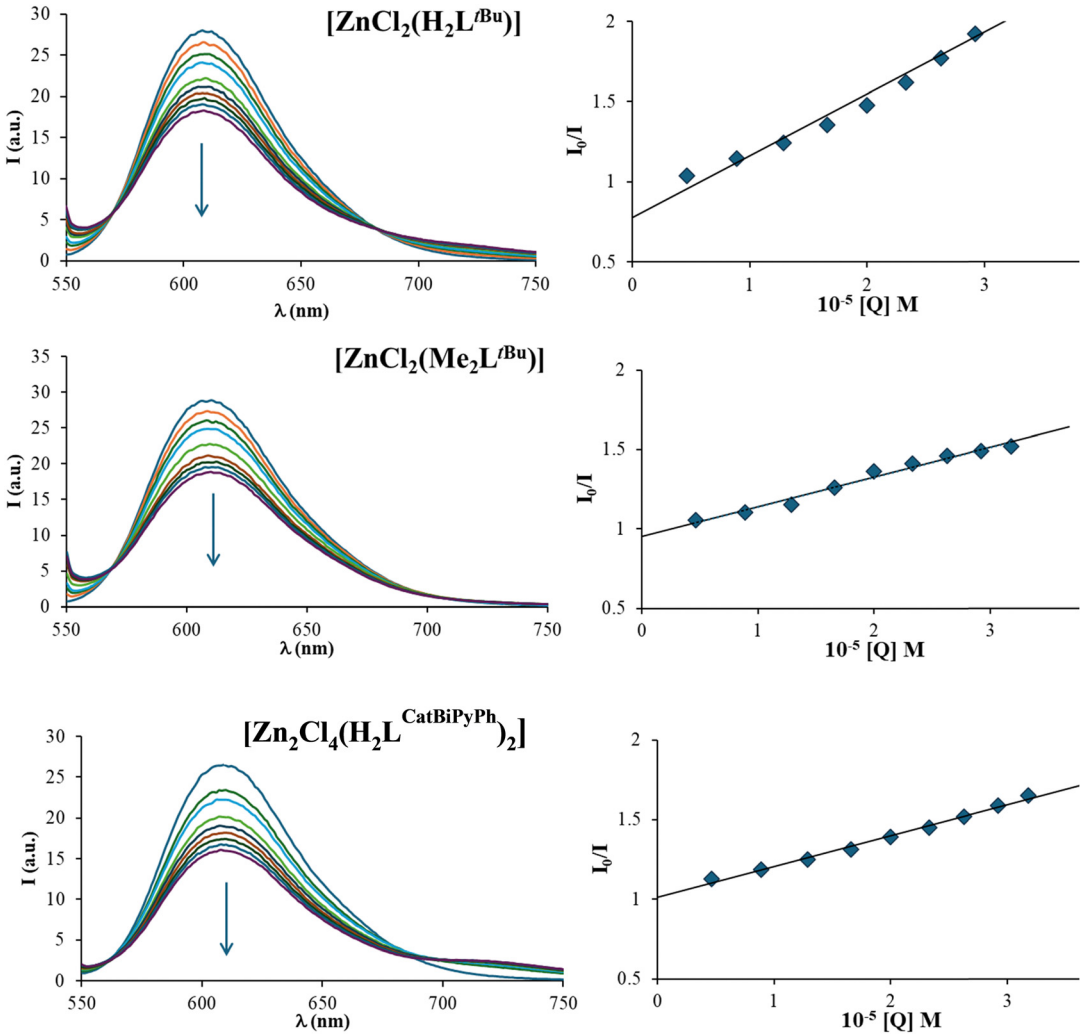

Fig. 4 Fluorescence titration spectra of EB/DNA solution (ratio EB : DNA was 1 : 1, 5 μM) in the absence and presence of the examined complexes. The arrow shows changes in the spectral band with the increasing complex concentration (added up to ratio 5). Inset graph: Stern–Volmer plots for CT-DNA/EB fluorescence titration in the presence of the examined complexes.

complex's potential to displace EB from the DNA-EB complex. The DNA-EB solution was prepared by combining solutions of EB and DNA (5 μM, pH = 7.4). The impact of complex binding to DNA was probed by monitoring changes in the fluorescence emission spectrum following the addition of the complex solution *p* to *a* ratio of 5.

The quenching constant, K_{sv}, is calculated from the slopes of straight lines obtained from the following Stern–Volmer equation (eqn (1)), and the obtained values are presented in Table 3.

$$I_0/I = 1 + K_{sv}[Q] \quad (1)$$

[Q] is the concentration of the complex, I_0 and I represent emission intensities in the absence and presence of the complex, and K_{sv} is the Stern–Volmer constant obtained from the slope of the I_0/I *vs.* [Q] plot.[37,38]

All examined complexes showed quenching constant, K_{sv}, values in the order of 10^4. Constant values follow the order of $[ZnCl_2(Me_2L^{tBu})] < [ZnCl_2(H_2L^{CatBiPyPh})] < [ZnCl_2(H_2L^{tBu})]$.

Table 3 Values of Stern–Volmer constants, K_{sv}, obtained using the Stern–Volmer equation and the number of binding sites, *n*, determined based on the Scatchard equation for the interaction of the examined complexes with human serum albumin, HSA

	DNA	HSA	
	10^4 K_{SV} [M^{-1}]	10^5 K_{SV} [M^{-1}]	*n*
$[ZnCl_2(H_2L^{tBu})]$	3.8 ± 0.1	2.4 ± 0.1	0.98
$[ZnCl_2(Me_2L^{tBu})]$	1.9 ± 0.1	0.5 ± 0.1	0.81
$[Zn_2Cl_4(H_2L^{CatBiPyPh})_2]$	2.1 ± 0.1	1.6 ± 0.1	0.69

Notably, the $[ZnCl_2(H_2L^{tBu})]$ complex exhibited a significantly higher compared to the other complexes, as indicated by K_{sv} constants, shown in Table 3.

Among these, the $[ZnCl_2(H_2L^{tBu})]$ complex displayed a notably higher K_{sv}, which can be attributed to distinct structural characteristics that impact its interaction with DNA. The structural difference in $[ZnCl_2(H_2L^{tBu})]$ lies in its inclusion of a less sterically demanding hydrogen atom, which minimally

Published on 07 February 2025. Downloaded by Universitat Erlangen Nurnberg on 2/7/2025 3:13:54 PM.

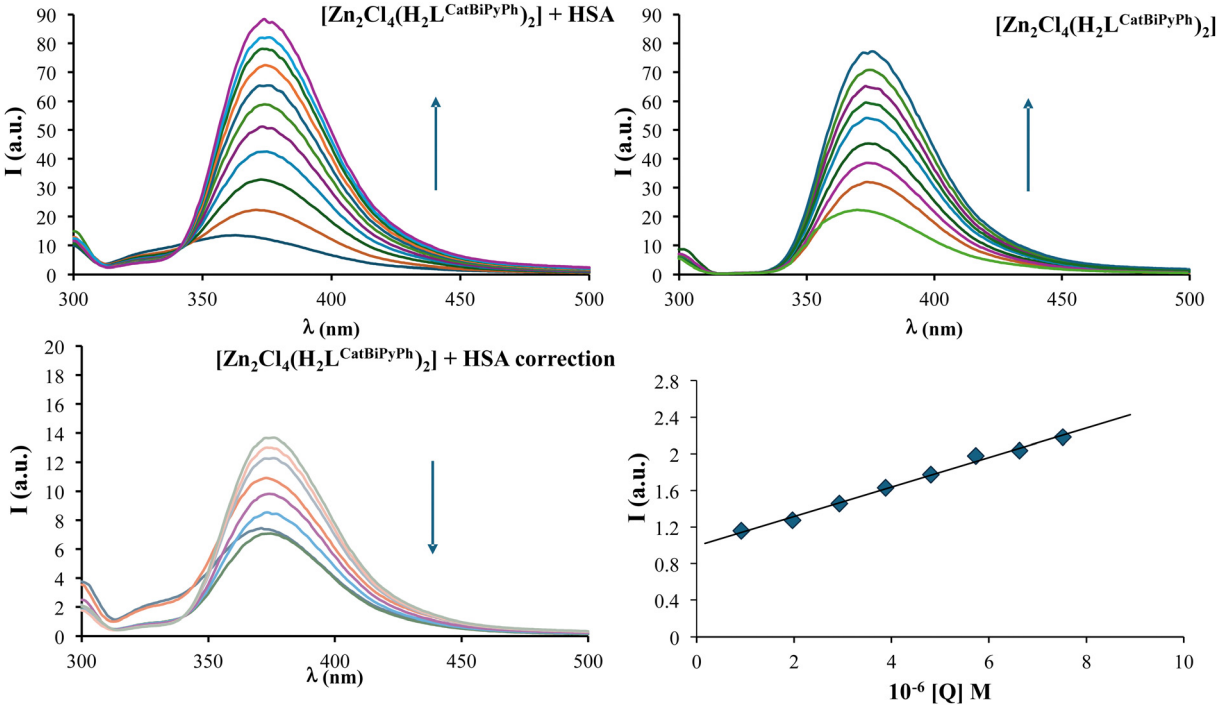

Fig. 5 Fluorescence titration spectra of HAS (2 μM) solution in the absence and presence of the examined complex **[ZnCl$_2$(H$_2$L^{CatBiPyPh})]**. The arrow shows changes in the spectral band with the increasing complex concentration (added up to ratio 5). Inset graph: Stern–Volmer plots for HSA fluorescence titration in the presence of the examined complex **[ZnCl$_2$(H$_2$L^{CatBiPyPh})]**.

obstructs the orientation of the complex. This reduced steric hindrance enhances its approachability towards the DNA molecule, enabling closer proximity and stronger interaction. In contrast, the more sterically hindered complexes **[ZnCl$_2$(Me$_2$L^{tBu})]** and **[ZnCl$_2$(H$_2$L^{CatBiPyPh})]** are less able to achieve such favorable positioning, resulting in lower K_{sv} constants.

This effect underscores the role of steric factors and molecular geometry in governing the binding affinities of metal complexes with biological molecules, particularly DNA. Understanding these structural influences provides insights into optimizing metal complexes for targeted DNA.

Protein binding investigations

Serum albumin, the predominant protein in blood circulation, plays a crucial role in the transport of drugs to their target sites. Investigating the interactions of the examined complexes with serum albumin is indispensable for elucidating the mechanism of action of anticancer drugs.

Fluorescence spectroscopy of HSA

The interaction between the investigated complexes and human serum albumin (HSA) was studied using fluorescence spectroscopy. Excitation of the HSA solution at 295 nm resulted in fluorescence originating from tryptophan residues. Upon addition of the complexes to the HSA solution, a noticeable increase in fluorescence intensity was observed, as depicted in Fig. 5 and Fig. S4 and S5 (ESI†). Concurrently, a series of spectra were recorded with increasing concentrations of the complexes in the absence of HSA, as shown in Fig. 5 and Fig. S4 and S5 (ESI†).

To isolate the fluorescence attributable to the complexes, corrections were applied to the fluorescence values of the HSA solution. The resulting corrected data, illustrated in Fig. 5 and Fig. S4 and S5 (ESI†), provided insights into the interaction dynamics. The Stern–Volmer constant (K_{sv}) for the complexes' interactions with serum albumin was calculated using the Stern–Volmer eqn (1), while the number of binding sites (n) was determined *via* the Scatchard eqn (2). Detailed values are listed in Table 3.

$$B/F = K(n - B) \quad (2)$$

where B and F are bound and free ligand concentrations, respectively, n is the binding capacity, and K is the association constant; when $B \ll n$ and when K is very large, the ratio B/F will appear to be constant.

The observed decrease in fluorescence can be ascribed to alterations in the tertiary structure of HSA, likely due to environmental changes around tryptophan residues upon complex binding to the protein.

Based on the obtained K_{sv} values given in Table 3, it can be observed that there is a moderate interaction between the examined complexes and HSA.

Cytotoxicity of zinc(II) complexes

The zinc complexes induced a significant decrease in the viability of colon (HCT-116) and pancreatic (MIA PaCa-2) cancer cell lines. A significant reduction in viability in both cell lines

 This journal is © The Royal Society of Chemistry and the Centre National de la Recherche Scientifique 2025

Published on 07 February 2025. Downloaded by Universitat Erlangen Nurnberg on 2/7/2025 3:13:54 PM.

Table 4 The cytotoxic effect of zinc(II) complexes expressed as IC_{50} value (μM) on colon (HCT-116) and pancreatic (MIA PaCa-2) cancer cell lines

Complexes	Cell line	24 h	72 h
$[ZnCl_2(H_2L^{tBu})]$	HCT-116	30.43 ± 1.25	25.79 ± 0.78
	MIA PaCa-2	34.36 ± 1.11	3.94 ± 0.22
$[ZnCl_2(Me_2L^{tBu})]$	HCT-116	75.23 ± 2.48	47.71 ± 1.51
	MIA PaCa-2	71.43 ± 3.98	12.1 1 ± 1.20
$[Zn_2Cl_4(H_2L^{CatBiPyPh})_2]$	HCT-116	121.24 ± 4.47	35.92 ± 2.32
	MIA PaCa-2	78.90 ± 1.92	26.31 ± 1.87
CDDP (cisplatin)	HCT-116	11.11 ± 0.13[a]	5.33 ± 0.4[a]
	MIA PaCa-2	3.47[b]	8.43 ± 1.89[c]

[a] Ref. 20. [b] Ref. 39. [c] Ref. 40.

implies that a cytotoxic effect of the treatment is present, which is expressed in IC_{50} values and shown in Table 4. The zinc(II) complex $[ZnCl_2(H_2L^{tBu})]$ exhibits a pronounced cytotoxic effect on both tested cell lines, with particularly strong activity observed after 72 hours in MIA PaCa-2 cells, surpassing the effects of cisplatin (Table 4).[39,40]

The observed binding affinities for CT-DNA and HSA, reflected by quenching constant (K_{sv}), exhibit a clear correlation with the *in vitro* cytotoxic effects of the zinc(II) complexes. Enhanced DNA binding, particularly for complexes such as $[ZnCl_2(H_2L^{tBu})]$, is likely to result in substantial disruption of DNA integrity and function, inducing processes like apoptosis or necrosis within the target cells. These effects correspond with the higher affinity of this complex for CT-DNA, which is associated with a more pronounced cytotoxic response in the tested cancer cell lines, particularly in the pancreatic cells. Conversely, complexes with weaker binding to DNA, such as $[ZnCl_2(Me_2L^{tBu})]$, demonstrate a relatively lower cytotoxicity. Additionally, the moderate binding interaction with HSA, as indicated by the K_{sv} values, implies that these complexes may achieve adequate bioavailability and distribution, allowing them to accumulate in cancerous tissues where they may exert enhanced therapeutic effects. These data underscore the pivotal role of both strong DNA binding and the interaction with serum proteins, which collectively contribute to the overall cytotoxic potential of these zinc(II) complexes in cancer treatment.

Cell death induction by zinc(II) complexes

The cytotoxic effect of zinc(II) complexes on colon HCT-116 and pancreatic carcinoma cells MIA PaCa-2 led to significant induction of apoptosis and necrosis through typical morphological changes (Fig. 6 and 7). In the case of the complex $[ZnCl_2(H_2L^{tBu})]$, the most significant occurrence of apoptosis is observed, while necrosis is present in a low percentage (Table 5). The highest percentage of necrosis was observed in the complex $[ZnCl_2(Me_2L^{tBu})]$ in both cell lines (Table 5).

Medicinal inorganic chemistry takes an important place in antitumor therapy-related research, due to the wide spectrum of compounds adapted and suitable for investigation.[41,42] Over the years, many metal complexes have been tested from this aspect. The first synthesized, tested, and included in clinical treatment, among organometallic complexes, was cisplatin.[43,44] Cisplatin has been used in treating various types of malignancy;

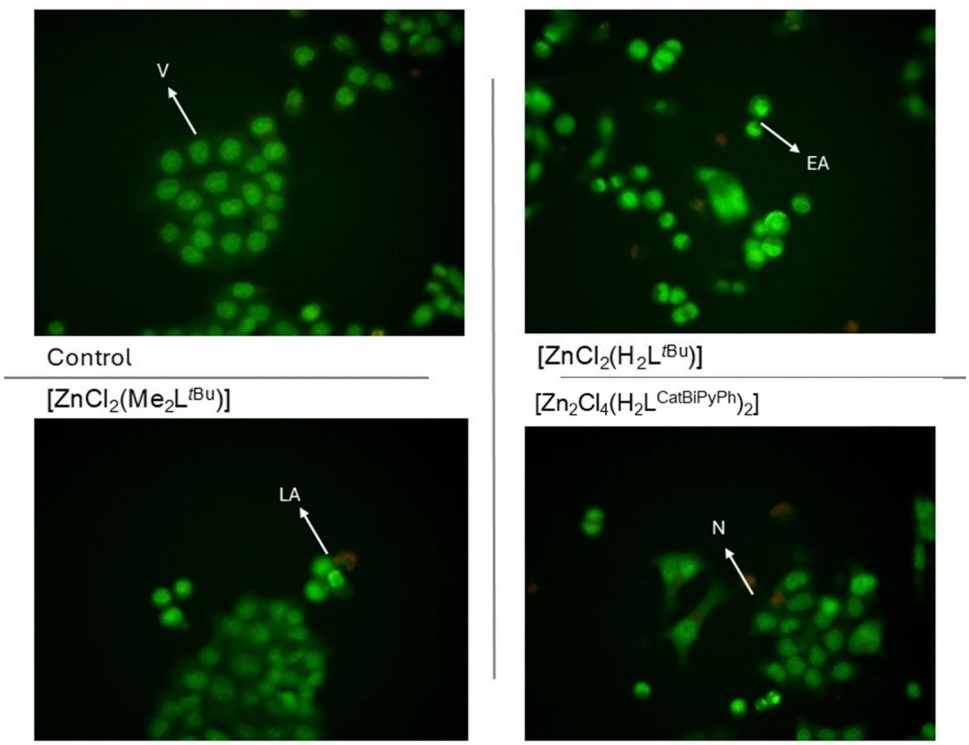

Fig. 6 Morphology of viable (V), apoptotic (early – EA and late – LA), and necrotic (N) HCT-116 cells under the influence of different zinc(II) complexes (concentration of 10 μM). Micrographs are made at a magnification of 400×.

Published on 07 February 2025. Downloaded by Universitat Erlangen Nurnberg on 2/7/2025 3:13:54 PM.

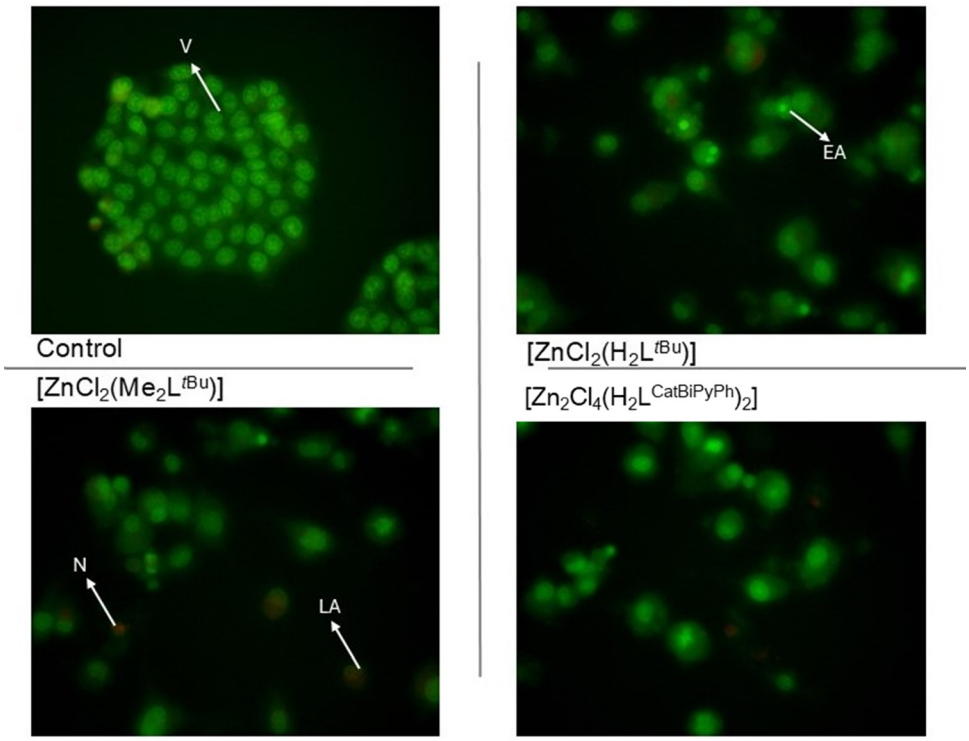

Fig. 7 Morphology of viable (V), apoptotic (early – EA and late – LA), and necrotic (N) MIA PaCa-2 cells under the influence of different zinc(II) complexes (concentration of 10 μM). Micrographs are made at a magnification of 400×.

Table 5 The percentage of viable, apoptotic and necrotic cells in the total number of control (nontreated) cancer cells (HCT-116 and MIA PaCa-2) and cells treated with zinc(II) complexes (10 μM), 24 h after treatment

Cell line	Complexes	Viable cells	Early apoptosis	Late apoptosis	Necrosis
HCT-116	Control	97.13 ± 2.52	2.87 ± 0.27	—	—
	$[ZnCl_2(H_2L^{tBu})]$	76.46 ± 0.41[a]	21.21 ± 0.54[a]	1.23 ± 0.21[a]	1.10 ± 0.07[a]
	$[ZnCl_2(Me_2L^{tBu})]$	86.32 ± 0.74[a]	7.28 ± 0.74[a]	3.45 ± 0.62[a]	2.9 5± 0.21[a]
	$[ZnCl_2(H_2L^{CatBiPyPh}]$	89.63 ± 0.49[a]	6.09 ± 1.03[a]	1.54 ± 0.95[a]	2.74 ± 0.41[a]
MIA PaCa-2	Control	98.23 ± 3.14	1.77 ± 0.21	—	—
	$[ZnCl_2(H_2L^{tBu})]$	72.01 ± 2.23[a]	20.77 ± 2.09[a]	6.46 ± 0.26[a]	0.76 ± 0.32[a]
	$[ZnCl_2(Me_2L^{tBu})]$	86.53 ± 2.15[a]	8.15 ± 2.68[a]	1.90 ± 0.15[a]	3.42 ± 0.79[a]
	$[ZnCl_2(H_2L^{CatBiPyPh}]$	84.40 ± 0.71[a]	10.49 ± 0.38[a]	3.12 ± 0.14[a]	1.98 ± 0.19[a]

The results are presented as the mean ± standard error of three independent experiments. [a] Statistically significant difference ($p < 0.05$) compared to control values.

however the noticeable antitumor effect of various organometallic complexes is limited by a series of side effects that occur during their use. This is the reason for intensified research in this field, to find an adequate complex with a suitable action. Among metal complexes, zinc(II) complexes stand out because zinc is the most abundant metal in our body, and thus the risk of being toxic to the body is reduced. However, their cytotoxicity on many cancer cell lines has been reported.[45,46]

Malignancy is the most common health problem today, and it is very difficult to establish an identical method of treatment for all types of cancer. For this reason, treating different model systems with certain treatments, in this case zinc(II) complexes, will give a more detailed view of the spectrum of their action. Colon and pancreatic cancers are some of the most aggressive types of cancer in the human gastrointestinal tract.[47,48] The results of our research showed that zinc(II) complexes lead to a significant cytotoxic effect on cell lines originating from these two carcinomas, HCT-116 originating from colon cancer and MIA PaCa-2 from pancreatic cancer. The complex **$[ZnCl_2(H_2L^{tBu})]$** exhibits greater effects than CDDP, which was used as a positive control cytostatic agent, on MIA PaCa-2 cells after 72 h. Considering the aggressiveness of this cancer,[7] long-term effects in reducing the cell viability and non-recovery of the cells from the treatment in prolonged time are the valuable results. Also, zinc(II) complexes showed a significant proapoptotic effect on the examined cell lines, which is considered a good mechanism of their action. It is known that zinc(II) complexes were combined with various phenols and flavonoids, so the zinc(II) complex with

 This journal is © The Royal Society of Chemistry and the Centre National de la Recherche Scientifique 2025

Published on 07 February 2025. Downloaded by Universitat Erlangen Nurnberg on 2/7/2025 3:13:54 PM.

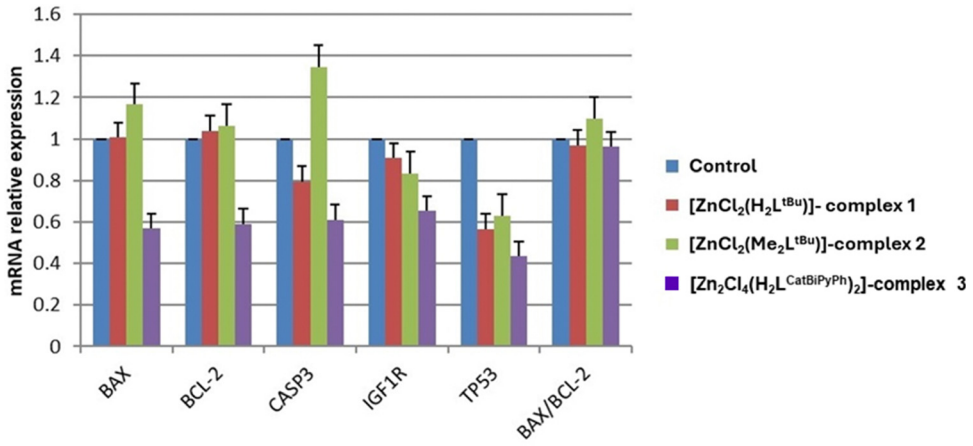

Fig. 8 Analysis of *Bax*, *Bcl-2*, *CASP3*, *IGF1R*, and *TP53* mRNA expression and *Bax/Bcl2* ratio 24 h after treatment. Gene expression levels were determined by qPCR and normalized to *ACTB*. Data represent mean ± sem.

quercetin was shown to induce apoptosis in HepG2 and HCT-116 cells.[49] Also, in the tested samples, necrosis occurred in a certain percentage. Still, it is noted that the necrosis rate is the lowest in the case of the action of the **[ZnCl$_2$(H$_2$L^{tBu})]** complex, which also shows the strongest cytotoxic effect. The **[ZnCl$_2$(H$_2$L^{tBu})]** complex stands out from the others due to the most favorable mode of action.

Analyses of gene expression levels

In order to elucidate the changes in apoptotic genes, the mRNA expression levels of *Bax (bcl-2*-like protein 4), *Bcl-2* (*B*-cell lymphoma 2), *CASP3* (Caspase 3), *IGF1R* (insulin-like growth factor 1), and *TP53* (homo sapiens tumor protein p53) genes were analyzed by quantitative real-time PCR 24 hours after treatment (Fig. 8).[50–52] Compared to the control untreated cells, the analysis showed a difference in the gene expression level between cells treated with different zinc complexes. All complexes showed a downregulation of the tumor suppressor *TP53* gene. This suggests that the observed activation of apoptosis is probably initiated through the p53 independent pathway as previously described.[53] Down regulation of *IGF1R* that resulted due to treatment with all complexes could indicate a decrease of cell proliferation and apoptotic pathway activation.[54] The higher expression of the *Bax* proapoptotic gene and *Bcl-2* antiapoptotic gene in **[ZnCl$_2$(Me$_2$L^{tBu})]**-treated samples could lead to necrosis by increasing cell damage (*Bax*) or inhibiting program cell death in damaged cells (*Bcl-2*).[55] **[ZnCl$_2$(H$_2$L^{tBu})]** treatment resulted due to downregulation of the tumor suppressor *CASP3*, which could interfere with an effective apoptotic process, as well as *IGF1R*, which can decrease cell proliferation indicating the importance of *TP53*-independent apoptotic pathways. **[ZnCl$_2$(H$_2$L^{CatBiPyPh})]** showed potential for lowering all investigated gene expression levels compared to the control cell line. The obtained results suggest that at the transcriptional level, complex mechanisms might be involved in the apoptotic/necrotic pathway activation caused by treatment of zinc complexes, which should be further analyzed at the post-transcriptional level in more detail and is beyond the scope of this study.

The mechanism of the biological activity of zinc(II) complexes could be linked to the ability of zinc(II) to adopt various coordination geometries (tetrahedral, square pyramidal, and octahedral), which allows it to interact effectively with diverse donor sites of nucleophiles.[18] The nature of the ligand in the inner coordination sphere plays a crucial role in the binding of the metal complexes to biomolecules and their cytotoxic effects.[18–22] Moreover, the square pyramidal structure enables the complex to coordinate donor atoms from various positions, ensuring that it can adapt to the specific conformations of the biomolecule it targets.[20,21] This adaptability is essential for inducing structural changes, such as DNA unwinding or enzyme inhibition, both of which contribute to the cytotoxic effects.

The ability of the zinc(II) complex to switch between different coordination states may also be critical in maintaining its bioactivity in the dynamic cellular environment.[18] Notably, the square pyramidal geometry around the zinc(II) ion facilitates coordination with different donor atoms, such as the N7 nitrogen or phosphate groups from nucleotides like 5′-GMP. This geometry enables the complex to form stable yet flexible interactions with nucleophilic sites, allowing the zinc(II) complex to effectively intercalate or bind to these molecules.[18,20,21] This connection between coordination geometry and biological activity underscores the importance of the ligand environment and structural flexibility in the antitumor properties of zinc(II) complexes.

Conclusions

Three novel Zn(II) complexes **[ZnCl$_2$(H$_2$L^{tBu})]**, **[ZnCl$_2$(Me$_2$L^{tBu})]** and **[Zn$_2$Cl$_4$(H$_2$L^{CatBiPyPh})$_2$]** were synthesized and characterized. The results obtained from X-ray analysis show that the complexes crystallize in the triclinic crystal system and the $P\bar{1}$ space group. Complex **[ZnCl$_2$(H$_2$L^{tBu})]** is five-coordinated with a tridentate *N*,*N*,*N*-donor ligand and two chlorido ligands, adopting a distorted trigonal bipyramidal geometry. On the other hand, **[Zn$_2$Cl$_4$(H$_2$L^{CatBiPyPh})$_2$]** consists of two parts related by an inversion center, and its formula is $Zn_2C_{14}C_{52}N_8O_4H_{44}\cdot 1.73H_2O$.

Published on 07 February 2025. Downloaded by Universitat Erlangen Nurnberg on 2/7/2025 3:13:54 PM.

The Zn(II) ion is four-coordinated by two nitrogen atoms and two chlorido ligands and the geometry surrounding the Zn(II) ion is a distorted tetrahedron. All examined complexes exhibited quenching constant, K_{sv}, values in the order of 10^4 with CT-DNA. Constant values followed the trend **[ZnCl$_2$(Me$_2$L^{tBu})]** < **[Zn$_2$Cl$_4$(H$_2$L^{CatBiPyPh})$_2$]** < **[ZnCl$_2$(H$_2$L^{tBu})]**. The results indicated a moderate interaction between the complexes and HSA. The zinc(II) complexes showed significant cytotoxic effects on colon (HCT-116) and pancreatic (MIA PaCa-2) cancer cell lines, particularly on pancreatic cells in prolonged time of treatment, 72 h. The observed cytotoxicity leads to marked apoptosis and necrosis, as indicated by typical morphological changes. Apoptosis was most pronounced with the complex **[ZnCl$_2$(H$_2$L^{tBu})]**, while necrosis occurred at lower levels. The gene expression level of apoptosis related genes emphasizes a complex mechanism behind activation of apoptotic/necrotic related signaling pathways which should be further investigated in future studies on both transcriptomic/proteomic levels and considering more genes/proteins involved in those processes.

Experimental

Chemicals

All reagents used in this study were of analytical grade or higher purity, obtained from Sigma-Aldrich (St. Louis, MO, USA), Acros Organics (Thermo Fisher Scientific, Geel, Belgium) and Merck (Darmstadt, Germany). The ligands 2,6-bis(5-*tert*-butyl-1*H*-pyrazol-3-yl)pyridine (H$_2$L^{tBu}), 2,6-bis(5-*tert*-butyl-1*H*-pyrazole-3-yl)pyridine (Me$_2$L^{tBu}) and 1,2(bis(5-phenyl-1*H*-pyrazole-3-yl)-metoxy)benzene (H$_2$L^{CatBiPyPh}) were prepared following the literature procedures.[56,57]

Instrumentation

The ^{1}H, ^{13}C and ^{1}H-^{1}H COSY spectra were acquired on Bruker Avance III 400 MHz and Bruker Avance Neo 500 MHz spectrometers. Elemental analyses were performed on a Carlo Erba Elemental Analyzer 1106. UV/Vis spectra were recorded using two double-beam UV/Vis spectrophotometers: the Uvikon XS (Secomam, Alès, France) and the PerkinElmer UV/Vis Lambda 35 (PerkinElmer Inc., Shelton, CT, USA). Both instruments are equipped with pre-aligned tungsten and deuterium lamps, a wavelength range of 190–1100 nm, a variable bandwidth range from 0.5 to 4 nm, and a 1 cm path length cell. IR data were obtained using a PerkinElmer® Spectrum One (PerkinElmer Inc., Shelton, CT, USA). Fluorescence measurements were carried out on a RF-1501 PC spectrofluorometer (Shimadzu, Japan). The excitation and emission bandwidths were both 10 nm. The pH measurements were recorded on a Jenway 4330 pH meter (Thermo Fisher Scientific,Waltham, MA, USA) with a combined Jenway glass microelectrode that had been calibrated with standard buffer solutions of pH 4.0, 7.0, and 10.0 (Merck).

General procedure for the synthesis

To a stirred 10 mL ethanolic solution of anhydrous $ZnCl_2$ (21 mg, 0.015 mmol), 10 mL ethanolic solution of ligands H$_2$L^{tBu} (5.0 mg, 0.015 mmol), Me$_2$L^{tBu} (5.2 mg, 0.015 mmol) and H$_2$L^{CatBiPyPh} (6.3 mg, 0.015 mmol) was added dropwise in a 1 : 1 ratio. The solution was stirred overnight at room temperature. Evaporation of solvent at room temperature resulted in the formation of white crystals. Spectra of the obtained complexes are present in the ESI† (Fig. S1–S3).

[ZnCl$_2$(H$_2$L^{tBu})]. Yield 49.9 mg (72.64%). Anal. calc. for $C_{19}H_{26}Cl_2N_5Zn$: N, 15.20; C, 49.53; H, 5.69. Found: N, 15.24; C, 49.73; H, 5.68. ^{1}H NMR (400 MHz, MeOD, 25 °C) 7.69 (s, HN–CC*H*C, 2H), 7.38 (m, *para*-Ar-C*H*, 1H), 7.14 (d, *meta*-Ar-C*H*, 1H), 6.98 (d, *meta*-Ar-C*H*, 1H), 5.19 (s, N*H*, 2H), 1.20 (s, C(CH_3)$_3$, 18 H) ppm. ^{13}C NMR (100 MHz, MeOD, 25 °C) 128.53 (HN–*C*CHC, 2C), 125.15 (HN–C*C*HC, 2C) 122.09 (*para*-Ar-*C*H, 1C), 115.95 (*meta*-Ar-*C*H, 2C), 102.06 (*ortho*-Ar-*C*, 2C) ppm. FT-IR (KBr, 4000–500 cm^{-1}): 3552 (N–H stretch); 2960 (C–H, stretch); 1615, 1515, 1462 (C=C, C–N), 790 (Zn–N).[18,58] UV-vis (CH$_3$OH, λ_{max}, nm): 330, 416.

[ZnCl$_2$(Me$_2$L^{tBu})]. Yield 59.6 mg (81.86%). Anal. calc. for $C_{21}H_{30}Cl_2N_5Zn$: N, 14.32; C, 51.60, H, 6.19. Found N, 14.28; C, 51.70; H, 6.21. ^{1}H NMR (400 MHz, MeOD, 25 °C) 7.96 (s, HN–CC*H*C, 2H), 8.50–8.21 (m, *ortho*-Ar-C*H*, *meta*-Ar-C*H*, 3H), 7.14 (s, *para*-Ar-C*H*, 1H), 6.93 (s, N*H*, 2H), 4.33 (s, NCH_3, 6H), 1.21 (s, C(CH_3)$_3$, 18 H). ^{13}C NMR (100 MHz, MeOD, 25 °C) 101.37 (CH$_3$N–C*C*HC, 2C), 56.92 (CH$_3$N–CCH*C*, 2C), 31.36 (N*C*H$_3$, 2C), 28.19 (*C*(CH$_3$)$_3$, 2C), 16.95(C(*C*H$_3$)$_3$, 6C). FT-IR (KBr, 4000–500 cm^{-1}): 3436 (N–H stretch); 2959 (C–H, stretch); 1608, 1575, 1458(C=C, C–N), 820 (Zn–N).[18,58] UV-vis (CH$_3$OH, λ_{max}, nm): 410.

[Zn$_2$Cl$_4$(H$_2$L^{CatBiPyPh})$_2$]. Yield 48.3 mg (57.83%). Anal. calc. for $C_{26}H_{23}Cl_2N_4O_2Zn$: N, 10.01; C, 55.79; H, 4.14; O, 5.72. Found: N, 10.05; C, 55.45, H, 4.16; O, 5.74. ^{1}H NMR (400 MHz, MeOD, 25 °C) 7.69 (s, HN–CC*H*C, 8H), 7.38 (m, *para*-Ar-C*H*, 4H), 7.13 (d, *meta*-Ar-C*H*, 4H), 6.93 (d, *meta*-Ar-C*H*, 1H), 5.19 (s, –CH_2, 6H) ppm. ^{13}C NMR (100 MHz, MeOD, 25 °C) 158.01 (Ar-*C*–O, 4C), 142.42 (Ar-*C*–pyrazole, 2C), 120.15 (Ar-*C*H, 4C), 119.57 (Ar-*C*H, 4C), 99.12 (C–*C*H–C, middle-Ar), 30.99 (C–*C*H–C, pyrazole 1C), 28.83 (C–*C*H–C, pyrazole 1C). FT-IR (KBr, 4000–500 cm^{-1}): 3292 (N–H stretch); 2919 (C–H, stretch); 1591, 1505, 1458 (C=C, C–N), 1259 (C–O), 765 (Zn–N).[18,58] UV-vis (CH$_3$OH, λ_{max}, nm): 412.

X-ray diffraction measurements

Two single crystals of compounds **[Zn$_2$Cl$_4$(H$_2$L^{CatBiPyPh})$_2$]** and **[ZnCl$_2$(H$_2$L^{tBu})]** were selected for the data collection under an optical microscope. For the diffraction experiments the crystals were coated with an oil-based cryoprotectant and mounted on cryoloops. Studies were conducted using Rigaku SuperNova XtaLAB (for **[ZnCl$_2$(H$_2$L^{CatBiPyPh})]**) and Rigaku XtaLAB Synergy-S (for **[ZnCl$_2$(H$_2$L^{tBu})]**) X-ray diffractometers, where the former is operated with a monochromatic micro-focus CuKα tube (λ = 1.54184 Å) at 50 kV and 1.0 mA and equipped with a CCD HyPix 3000 hybrid photon counting detector, and the latter is operated with the monochromatic micro-focus CuKα tube PhotoJet-S (λ[CuKα] = 1.54184 Å) at 50 kV and 1.0 mA and equipped with a CCD HyPix 6000HE hybrid photon counting detector. All data collection strategies were designed to collect more than half of

 This journal is © The Royal Society of Chemistry and the Centre National de la Recherche Scientifique 2025

Published on 07 February 2025. Downloaded by Universitat Erlangen Nurnberg on 2/7/2025 3:13:54 PM.

Table 6 Crystallographic data, data collection and refinement parameters of the crystal structures of **[$Zn_2Cl_4(H_2L^{CatBiPyPh})_2$]** (CCDC number 2339722) and **[$ZnCl_2(H_2L^{tBu})$]** (CCDC number 2339723)

Compound	**[$ZnCl_2(H_2L^{CatBiPyPh})$]**	**[$ZnCl_2(H_2L^{tBu})$]**
Crystallographic data		
Formula	$Zn_2Cl_4C_{52}N_8O_4H_{44}\cdot 1.73H_2O$	$ZnCl_2C_{19}N_5H_{25}\cdot 2.46H_2O$
Space group	$P\bar{1}$	$P\bar{1}$
a [Å]	10.2771(4)	10.0761(4)
b [Å]	10.7950(3)	11.1556(5)
c [Å]	13.1138(4)	11.5131(4)
α [°]	103.771(3)	67.436(3)
β [°]	109.047(3)	84.168(3)
γ [°]	102.951(3)	75.427(4)
V [Å^3]	1261.45(8)	1156.60(9)
Z	1	2
Calculated density [g cm^{-3}]	1.51	1.45
μ [mm^{-1}]	3.56	3.82
Data collection parameters		
Angle range 2θ [°]	7.58–143.74	8.32–160.38
Index range	$-12 \le h \le 12$, $-13 \le k \le 13$, $-16 \le l \le 16$	$-12 \le h \le 12$, $-14 \le k \le 13$, $-14 \le l \le 12$
Total reflections, unique reflections and reflections with $F^2 > 2\sigma(F^2)$	13 634, 4885, 4260	15 818, 4845, 4272
R_{int}, R_σ	0.041, 0.046	0.043, 0.044
Refinement parameters		
R_1 [$F^2 > 2\sigma(F^2)$], wR_2 [$F^2 > 2\sigma(F^2)$]	0.0398, 0.1049	0.0317, 0.0767
R_1 and wR_2 (all data)	0.0489, 0.1117	0.0370, 0.0792
S	1.106	1.068
ρ_{max}, ρ_{min} [e$^-$ Å^{-3}]	0.52, −0.61	0.49, −0.50
CCDC	2339722	2339723

the Ewald sphere. Frame widths were 0.5 s. CrysAlisPro software was used for the integration and correction of diffraction data for polarization, for background and Lorentz effects, and for an empirical absorption correction based on spherical harmonics implemented in the SCALE3 ABSPACK algorithm.[59] The unit cell parameters were refined using a least-squares technique. The structure was solved using a dual-space algorithm and refined using SHELX programs, which were incorporated in the OLEX2 program package.[60–62] The carbon- and nitrogen-bound H atoms were placed in calculated positions and were included in the refinement in the "riding" model approximation, with C–H and N–H bond length of 0.95 Å and 0.88 Å, respectively, whereas a C–H bond length of CH_3 groups of **[$ZnCl_2(H_2L^{tBu})$]**) was fixed at 0.98 Å. The U_{iso}(H) parameters were fixed at 1.5U_{eq}(C) for the *tert*-butyl groups, whereas the U_{iso}(H) parameters were fixed at 1.2U_{eq}(C) and 1.2U_{eq}(N) for the rest of the C–H and N–H bonds. The structure of **[$ZnCl_2(H_2L^{tBu})$]** showed large residual peaks in the electron density near chlorine atoms. A careful analysis of the distances and angles between these peaks did not reveal any values that were close to the molecules of ethanol used in the synthesis. This is further evidence that ethanol molecules are not present in the structure, as the electron density values for these residual peaks do not correspond to any proposed disordering scheme. Therefore, these peaks were assigned to disordered H_2O molecules. This was later confirmed indirectly by significantly increased convergence factors and well-established anisotropic displacement parameters, as well as a reasonable disordering model. The positions of the hydrogen atoms of H_2O molecules were determined from the difference Fourier map and were included in the refinement using a "riding" model approximation with U_{iso}(H) set to 1.5U_{eq}(O), O–H bond lengths of 0.96 Å, and a H···H distance of 1.52 Å. Crystallographic data, data collection and refinement parameters as well as the corresponding CCDC numbers are listed in Table 6.

CT-DNA binding interactions

Fluorescence quenching studies. The binding affinity of the studied complexes with CT-DNA through intercalation was determined *via* fluorescence spectroscopy. All measurements were conducted at room temperature in a 0.01 M phosphate buffer solution at pH 7.4. Fluorescence measurements were made by adding increasing concentrations of the complex (0–50 μM) to a solution containing CT-DNA and EB. Each system was shaken at room temperature prior to measurement. Fluorescence intensity was measured with an excitation wavelength of 527 nm and an emission wavelength of 612 nm. The excitation and emission slit widths were both set to 10 nm, and the scan rate was maintained consistently. Emission spectra were recorded between 550 nm and 750 nm. The interaction between the complex and CT-DNA was investigated in the presence of ethidium bromide (EB) to evaluate the complex's potential to displace EB from the DNA-EB complex.[63,64]

HSA binding interactions. The binding affinity of the examined complexes with HSA was determined through fluorescence quenching experiments. Experiments were conducted at room temperature in a 0.01 M phosphate buffer solution at pH 7.4. The HSA concentration was maintained at 2 μM, while the complex concentration varied from 0 to 30 μM, resulting in a marked decrease in emission at 352 nm. Each sample was shaken at room temperature before measurement. Fluorescence intensity was measured at an excitation wavelength of 295 nm, with emissions recorded in the 300 to 500 nm range.

Published on 07 February 2025. Downloaded by Universitat Erlangen Nurnberg on 2/7/2025 3:13:54 PM.

Both the excitation and emission slit widths were set to 10 nm, and the scan rate was maintained consistently. The Stern–Volmer constants (K_{sv}) were determined using Stern–Volmer eqn (2).[65,66]

Cell line culturing. The human colorectal cancer cell line HCT-116 and a human pancreas carcinoma cell line MIA PaCa-2 (obtained from the American Type Culture Collection, USA) were used for experimental analysis. Both cell lines are cultured in DMEM (Dulbecco's modified eagle medium, obtained from Capricorn, Germany) under standard conditions.[67]

Cell viability assay. The influence of different zinc(II) complexes on HCT-116 and MIA PaCa-2 cell viability was investigated, by measuring the intensity of purple formazan in control (only DMEM) and treated cell samples (MTT assay). Tetrazolium salt (3-[4,5-dimethylthiazol-2-yl]-2,5-diphenyltetrazolium bromide) was obtained from SERVA, Germany. The assay procedure was primarily described in the lilterature,[68] where we seeded 10^4 cells per well (96-well plate) and treated with different zinc(II) complexes in the 1–200 μM concentration range. The cell viability was measured for two time periods, 24 and 72 h. After reading on ELISA, the results are calculated as a ratio between the absorbance of treated and untreated cells, multiplied by 100, and from the viability curve. The IC_{50} values were obtained (by the CalcuSyn program) to measure cytotoxicity.

Type of induced cell death. The type of cell death induced by different zinc(II) complexes was determined by the fluorescent dye acridine orange (AO, obtained from Acros Organics, New Jersey, USA), and ethidium bromide (EB, obtained from SERVA, Germany).[69] For the experiment, 10^4 cells per well (96-well plate) were seeded, and treated with a concentration of 10 μM by different zinc(II) complexes. The morphological changes were monitored by staining with 10 μL of AO and EB dye per sample, 24 h after treatment. The number of cells in apoptosis and necrosis was proportionally determined based on the total number of cells (a minimum of 300 cells per sample). Detection was performed using a Nikon Ti-Eclipse fluorescence microscope.

RNA extraction and cDNA synthesis. Cell line HCT-116 was seeded into 6-well plates at a density of 1.5×10^4 cells per well. Cells were grown for several days until reaching a confluency greater than 80%. The cells were treated with three different complexes and incubated for 24 hours. For analysis, the cells were harvested with trypsin, centrifuged (10 min at 2000 rpm), and resuspended in PBS. Before RNA isolation, the cells were centrifuged for 10 minutes at 1500 rcf. Total RNA was isolated from the pelleted cells using the TRI REAGENT® BD kit (Sigma-Aldrich, St. Louis, USA). The quality and quantity of RNA were evaluated using a BioSpec-nano spectrophotometer (Shimadzu Scientific Instruments). Two micrograms of total RNA were used for complementary DNA (cDNA) synthesis using random primers. The conversion was performed by MultiScribeTM Reverse Transcriptase (50 U μL^{-1}) as part of the High-Capacity cDNA Reverse Transcription kit (Applied Biosystems). The final volume of the reaction was 20 μL, and the conversion was performed using the following program: 25 °C for 10 min, 37 °C for 120 min, and inactivation at 85 °C for 5 min. The generated cDNA was used as a template for gene expression analysis using quantitative real-time PCR (qRT-PCR).

Quantitative real time PCR (qRT-PCR). The mRNA levels of *Bax* (RefSeq. NM_001291428.1), *Bcl*2 (RefSeq. NM_000633.2), CASP3 (RefSeq. NM_004346), TP53 (RefSeq. NM_000546.6) and *IGF1R* (RefSeq. NM_000875.4) were evaluated using quantitative real-time PCR (qRT-PCR) with TaqMan® Gene Expression Assays and TaqMan® Gene Expression Master Mix (Applied Biosystems). Gene expression analysis was performed on LightCycler®480 II (Roche Diagnostics). Each amplification had a non-template control and an endogenous actin beta control (ACTB, RefSeq. NM_001101.3) to exclude variations arising from different inputs of total mRNA to the reaction. The real-time PCR conditions included an initial denaturation step at 95 °C for 10 min which was followed by 40 cycles of denaturation (15 s at 95 °C) and annealing/extension (1 min at 60 °C). The final reaction volume was 10 μL. Each sample was analyzed in duplicate, and the fluorescence level of the double-stranded DNA was monitored in real time. The classical ΔΔCt method was employed for data analysis, and the results were presented as mean fluorescence expressed in relative units. The corresponding non-treated cells were used as control.[45–47]

Author contributions

Rušid Hasić: investigation, validation. Majda Kolenović Serezlić: writing–original draft. Angelina Caković: investigation, validation, formal analysis, writing – original draft. Jovana Bogojeski: validation, formal analysis, writing – original draft. Danijela Nikodijević: investigation, validation, formal analysis, writing – original draft. Milena Milutinović: investigation, validation, formal analysis, writing – original draft. Aleksandra Stanojević: investigation, validation, formal analysis, writing – original draft. Milena Čavić: investigation, validation, formal analysis, writing – original draft. Andrei V. Egorov: software, formal analysis, writing – original draft. Andrei V. Komolkin: software, formal analysis, writing – original draft. Ilya V. Kornyakov: investigation, validation, writing – original draft. Andreas Scheurer: investigation, writing – review and editing. Ralph Puchta: software, writing – review and editing. Tanja V. Soldatović: conceptualization, methodology, investigation, supervision, writing – review and editing.

Data availability

The ESI† contains: Synthetic and analytical data for all new compounds; images of spectra for all new compounds; X-ray crystallographic information for structurally characterized species; computational details. Crystallographic Information Files (CIFs) are freely available from the CCDC (numbers 2339722 and 2339723).†

Conflicts of interest

There are no conflicts to declare

 This journal is © The Royal Society of Chemistry and the Centre National de la Recherche Scientifique 2025

Published on 07 February 2025. Downloaded by Universitat Erlangen Nurnberg on 2/7/2025 3:13:54 PM.

Acknowledgements

T. Soldatović and M. Kolenović Serezlić gratefully acknowledge financial support from the State University of Novi Pazar, Republic of Serbia. T. Soldatović, D. Nikodijević, M. Milutinović, and M. Čavić gratefully acknowledge financial support from the Ministry of Science, Technological Development and Innovation of the Republic of Serbia (Agreements No. 451-03-65/2024-03/200252, 451-03-66/2024-03/200122, 451-03-65/2024-03/200122 and 451-03-66/2024-03/200043). X-ray diffraction and NMR measurements were carried out at the Center for X-ray Diffraction Methods and Magnetic Resonance Research Center of Research Park of St. Petersburg State University. A.V. Egorov acknowledges support from Saint-Petersburg State University grant 104236506.

References

1 U. Sliwinska, F. P. Pruchnik, I. Pelinska, S. Ułaszewski, A. Wilczok and A. Zajdel, *J. Inorg. Biochem.*, 2008, **102**, 1947–1951.
2 M. Cwikowska, F. P. Pruchnik, R. Starosta, H. Chojnacki, A. Wilczok and S. Ułaszewski, *Inorg. Chim. Acta*, 2010, **363**, 2401–2408.
3 R. F. M. Frade, N. R. Candeias, C. M. M. Duarte, V. Andre, M. T. Duarte, P. M. P. Gois and C. A. M. Afonso, *Bioorg. Med. Chem. Lett.*, 2010, **20**, 3413–3415.
4 D. E. Morrison, J. B. Aitken, M. D. de Jonge, F. Issa, H. H. Harris and L. M. Rendina, *Chem. – Eur. J.*, 2014, **20**, 16602–16612.
5 H. Huang, P. Zhang, H. Chen, L. Ji and H. Chao, *Chem. – Eur. J.*, 2015, **21**, 715–725.
6 B. Read and P. Sylla, *Clin. Colon Rectal. Surg.*, 2020, **33**(5), 298–304.
7 Z. Zhao and W. Liu, *Technol. Cancer Res. Treat.*, 2020, **19**, 1–13.
8 Y. Xi and P. Xu, *Transl. Oncol.*, 2021, **14**(10), 101174.
9 M. Porchia, M. Pellei, F. Del Bello and C. Santini, *Molecules*, 2020, **24**, 5814.
10 H. Haase and L. Rink, *Metallomics*, 2014, **6**, 1175–1180.
11 V. Kolenko, E. Teper, A. Kutikov and R. Uzzo, *Nat. Rev. Urol.*, 2013, **10**, 219–226.
12 A. S. Nakashima and R. H. Dyck, *Brain Res. Rev.*, 2009, **59**, 347–373.
13 B. K. Bitanihirwe and M. G. Cunningham, *Synapse*, 2009, **63**, 1029–1049.
14 R. Crichton, In Chapter 12–Zinc–Lewis Acid and Gene Regulator, ed. Crichton R., *Biological Inorganic Chemistry*, 3rd edn Academic Press, Cambridge, MA, USA, 2019, pp. 339–362.
15 M. Hashemi, S. Ghavami, M. Eshraghi, E. P. Booy and M. Los, *Eur. J. Pharmacol.*, 2007, **557**, 9–19.
16 A. Steinbrueck, A. C. Sedgwick, J. T. Brewster, K. C. Yan, Y. Shang, D. M. Knoll, G. I. Vargas-Zuniga, X. P. He, H. Tian and J. L. Sessler, *Chem. Soc. Rev.*, 2020, **49**, 3726–3747.
17 R. B. Franklin, J. Zou, Y. Zheng, M. J. Naslund and L. C. Costello, *Int. J. Cancer Clin. Res.*, 2016, **3**, 037.
18 T. V. Soldatović, E. Selimović, B. Šmit, D. Ašanin, N. S. Planojević, S. D. Marković, R. Puchta and B. M. Alzoubi, *J. Coord. Chem.*, 2019, **72**, 690–706.
19 T. V. Soldatović, *Application of the Principle of Hard and Soft Acids and Bases to Mechanisms of Bioinorganic Reaction*, Livre de Lyon Publisher, Lyon, France, 2019.
20 T. V. Soldatović, E. Selimović, N. Milivojević, M. Jovanović and B. Šmit, *Appl. Organomet. Chem.*, 2020, **34**, e5864.
21 T. Soldatović, B. Šmit, E. M. Mrkalić, S. L. Matić, R. M. Jelić, M. Ćendić Serafinović, N. Gligorijević, M. Čavić, S. Aranđelović and S. Grgurić-Šipka, *J. Inorg. Biochem.*, 2023, **240**, 112100.
22 M. Kolenović Serezlić, R. Hasić, D. Ašanin, B. Šmit, S. L. Matić, M. Ćendić Serafinović, D. Nikodijević, C. J. Jovankić, S. Grgurić- Šipka and T. Soldatović, *Appl. Organomet. Chem.*, 2024, e7413.
23 Ž. D. Bugarčić, J. Bogojeski and R. van Eldik, *Coord. Chem. Rev.*, 2015, **292**, 91–106.
24 J. Korzekwa, A. Scheurer, F. W. Heinemann and K. Meyer, *Dalton Trans.*, 2017, **46**, 13811–13823.
25 S. Radisavljević, I. Bratsos, A. Scheurer, J. Korzekwa, R. Masnikosa, A. Tot, N. Gligorijević, S. Radulović and A. Rilak Simović, *Dalton Trans.*, 2018, **47**, 13696–13712.
26 M. M. Milutinović, J. V. Bogojeski, O. Klisurić, A. Scheurer, S. K. C. Elmorth and Ž. D. Bugarčić, *Dalton Trans.*, 2016, **45**, 15481–15491.
27 D. Lazić, A. Scheurer, D. Ćoćić and J. Milovanović, *Dalton Trans.*, 2021, **50**, 7686–7704.
28 A. Z. Petrović, D. C. Ćoćić, D. Bockfeld, M. Živanović, N. Milivojević, K. Virijević, N. Janković, A. Scheurer, M. Vraneš and J. V. Bogojeski, *Inorg. Chem. Front.*, 2021, **11**, 2749–2770.
29 D. Ćoćić, S. Jovanović, S. Radisavljević, J. Korzekwa, A. Scheurer, R. Puchta, D. Baskić, D. Todorović, S. Popović, S. D. Matić and B. Petrović, *J. Inorg. Chem.*, 2018, **189**, 91–102.
30 A. W. Addison, T. N. Rao, J. Reedijk, J. van Rijn and G. C. Verschoor, *J. Chem. Soc., Dalton Trans.*, 1984, **7**, 1349–1356.
31 O. Novakova, H. Chen, O. Vrana, A. Rodger, P. J. Sadle and V. Brabec, *Biochemistry*, 2003, **42**, 11544–11554.
32 M. A. Rizvi, M. Zaki, M. Afzal, M. Mane, M. Kumar, B. A. Shah, S. Srivastav, S. Srikrishna, G. M. Peerzada and S. Tabassum, *Eur. J. Med. Chem.*, 2015, **90**, 876–888.
33 A. Petrović, M. M. Milutinović, E. T. Petri, M. Živanović, N. Milivojević, R. Puchta, A. Scheurer, J. Korzekwa, O. R. Klisurić and J. Bogojeski, *Inorg. Chem.*, 2019, **58**, 307–319.
34 M. M. Milutinović, J. V. Bogojeski, O. Klisurić, A. Scheurer, S. K. C. Elmroth and Ž. D. Bugarčić, *Dalton Trans.*, 2016, **45**, 15481–15491.
35 A. Z. Petrović, D. C. Ćoćić, D. Bockfeld, M. Živanović, N. Milivojević, K. Virijević, N. Janković, A. Scheurer, M. Vraneš and J. V. Bogojeski, *Inorg. Chem. Front.*, 2021, **8**, 2749–2770.

Published on 07 February 2025. Downloaded by Universitat Erlangen Nurnberg on 2/7/2025 3:13:54 PM.

36 J. M. Kelly, A. B. Tossi, D. J. McConnell and C. Oh Uigin, *Nucleic Acids Res.*, 1985, **13**, 6017–6034.
37 B. C. Boger, B. E. Fink, S. R. Brunette, W. C. Tse and M. P. Hedrick, *J. Am. Chem. Soc.*, 2001, **123**, 5878–5891.
38 F. Dimiza, S. Fountoulaki, A. N. Papadopoulos, C. A. Kontogiorgis, V. Tangoulis, C. P. Raptopoulou, V. Psycharis, A. Terzis, D. P. Kessissoglou and G. Psomas, *Dalton Trans.*, 2011, **40**, 8555–8668.
39 B. Zhao, C. Qin, Z. Li, Y. Wang, T. Li, H. Cao, X. Yang, T. Li and W. Wang, *Cancer Cell Int.*, 2022, **22**, 374.
40 P. P. Che, A. K. Mapanao, A. Gregori, M. L. Ermini, A. Zamborlin, M. Capula, D. Ngadimin, B. J. Slotman, V. Voliani, P. Sminia and E. Giovannetti, *Cancers*, 2022, **14**(12), 3034.
41 R. Paprocka, M. Szadkowska, S. Janciauskiene, T. Kosmalski, M. Kulik and A. Helmin-Basa, *Coord. Chem. Rev.*, 2022, **452**, 214307.
42 A. Peacock and P. Sadler, *Chem. – Asian J.*, 2008, **3**, 1890–1899.
43 A. M. P. Romani, *Biochem. Pharmacol.*, 2022, **206**, 115323.
44 S. Ghosh, *Bioorg. Chem.*, 2019, **88**, 102925.
45 M. Pellei, F. Del Bello, M. Porchia and C. Santini, *Coord. Chem. Rev.*, 2021, **445**, 214008.
46 R. Vučelj, R. Hasić, D. Ašanin, B. Šmit, A. Caković, J. Bogojeski, M. Ć. Serafinović, B. S. Marković, B. Stojanović, S. Pavlović, I. Stanisavljević, I. Ćorović, M. D. Stojanović, I. Jovanović, T. Soldatović and B. Stojanović, *Int. J. Mol. Sci.*, 2024, **25**, 3027.
47 B. Read and P. Sylla, *Clin. Colon Rectal. Surg.*, 2020, **33**, 298–304.
48 J. X. Hu, C. F. Zhao, W. B. Chen, Q. C. Liu, Q. W. Li, Y. Y. Lin and F. Gao, *World J. Gastroenterol.*, 2021, **27**(27), 4298–4321.
49 M. Nakamura, D. Urakawa, Z. He, I. Akagi, D. X. Hou and K. Sakao, *Int. J. Mol. Sci.*, 2023, **24**, 1745.
50 H. E. Marei, A. Althani, N. Afifi, A. Hasan, T. Caceci, G. Pozzoli, A. Morrione, A. Giordano and C. Cenciarelli, *Cancer Cell Int.*, 2021, **21**(1), 703.
51 M. Zhou, X. Liu, Z. Li, Q. Huang, F. Li and C. Y. Li, *Int. J. Cancer*, 2018, **143**(4), 921.
52 E. Alfaro-Arnedo, I. P. López, S. Piñeiro-Hermida, M. Canalejo, C. Gotera, J. Sola, A. Roncero, G. Peces-Barba, C. Ruíz-Martínez and J. G. Pichel, *Oncogene*, 2022, **41**, 3625.
53 S. N. Bae, K. H. Lee, J. H. Kim, S. J. Lee and L. O. Park, *Biochem. Biophys. Res. Commun.*, 2017, **484**(1), 218.
54 G. Xu, J. Chu, Y. Shi, L. Huang and J. Fu, *J. Growth Horm. IGF Res.*, 2022, **66**, 101499.
55 N. Shinoura, Y. Yoshida, A. Asai, T. Kirino and H. Hamada, *Oncogene*, 1999, **18**, 5703.
56 J. Korzekwa, A. Scheurer, F. W. Heinemann and K. Meyer, *Dalton Trans.*, 2017, **46**, 13811.
57 R. W. Saalfrank, A. Scheurer, R. Puchta, F. Hampel, H. Maid and F. W. Heinemann, *Angew. Chem., Int. Ed.*, 2007, **46**, 269.
58 A. Lagutschenkov, U. J. Lorenz and O. Dopfer, *Int. J. Mass Spectrom.*, 2011, **308**, 316–329.
59 *CrysAlisPro, Version 1.171.41.94a*, Rigaku Oxford Diffraction, 2021.
60 G. M. Sheldrick, *Acta Crystallogr.*, 2015, **A71**, 3–8.
61 G. M. Sheldrick, *Acta Crystallogr.*, 2015, **C71**, 3–8.
62 O. V. Dolomanov, L. J. Bourhis, R. J. Gildea, J. A. K. Howard and H. Puschmann, *J. Appl. Cryst.*, 2009, **42**, 339–341.
63 F. Dimiza, F. Perdih, V. Tangoulis, I. Turel, D. P. Kessissoglou and G. Psomas, *J. Inorg. Biochem.*, 2011, **105**, 476–489.
64 K. Rippe, *B. I. F. Futura*, 1997, **12**, 20–26.
65 X. Q. Jonathan and B. Chaires, *Methods Enzymol.*, 2000, **321**, 353–369.
66 D. Senthil Raja, N. S. P. Bhuvanesh and K. Natarajan, *Inorg. Chem.*, 2011, **50**, 12852–12866.
67 M. G. Milutinović, V. M. Maksimović, D. M. Cvetković, D. D. Nikodijević, M. S. Stanković, M. Pešić and S. D. Marković, *J. Ethnopharmacol.*, 2019, **240**, 111951.
68 T. Mosmann, *J. Immunol. Methods*, 1983, **65**, 55–63.
69 D. Baskić, S. Popović, P. Ristić and N. N. Arsenijević, *Cell Biol. Int.*, 2006, **30**, 924.

 This journal is © The Royal Society of Chemistry and the Centre National de la Recherche Scientifique 2025